Review

Progress in Cellulose-Based Polymer Ionic Conductors: From Performance Optimization to Strain-Sensing Applications

Rouyi Lu [1], Yinuo Wang [2], Hao Pang [1], Panpan Zhang [2],* and Qilin Hua [1],*

[1] School of Integrated Circuits and Electronics, Beijing Institute of Technology, Beijing 100081, China
[2] College of Materials Science and Technology, Beijing Forestry University, Beijing 100083, China
* Correspondence: zhangpanpan2024@bjfu.edu.cn (P.Z.); huaqilin@bit.edu.cn (Q.H.)

Abstract

Intrinsically stretchable polymer ionic conductors (PICs) hold significant application prospects in fields such as flexible sensors, energy storage devices, and wearable electronic devices, serving as promising solutions to prevent mechanical failure in flexible electronics. However, the development of PICs is hindered by an inherent trade-off between mechanical robust and electrical properties. Cellulose, renowned for its high mechanical strength, tunable chemical groups, abundant resources, excellent biocompatibility, and remarkable recyclability and biodegradability, offers a powerful strategy to decouple and enhance mechanical and electrical properties. This review presents recent advances in cellulose-based polymer ionic conductors (CPICs), which exhibit exceptional design versatility for flexible electrodes and strain sensors. We systematically discuss optimization strategies to improve their mechanical properties, electrical conductivity, and environmental stability while analyzing the key factors such as sensitivity, gauge factor, strain range, response time, and cyclic stability, where strain sensing refers to a technique that converts tiny deformations (i.e., strain) of materials or structures under external forces into measurable physical signals (e.g., electrical signals) for real-time monitoring of their deformation degree or stress state.

Keywords: cellulose; polymer ionic conductors; hydrogels; ionogels; all-solid-state ionic conductors

1. Introduction

The rapid advancement of information technology have unveiled tremendous application prospects for flexible and stretchable electronics, including sensors, energy storage devices, and wearable systems [1]. Stretchable electrodes, as key components in these devices, are required to possess high electrical conductivity, excellent stretchability, and robust environmental stability. Traditional stretchable electronic conductors often suffer from disrupted conductive pathways under large strains due to a lack of intrinsic stretchability [2]. In contrast, polymeric ionic conductors (PICs) achieve conductivity through ion transport along and between polymer chains—a mechanism that remains effective even upon significant deformation, granting them intrinsic stretchability. Composed of a polymer network and dispersed ions, PICs enable efficient ion migration and charge transport [3]. Through tailored molecular design, they can be engineered to possess multifunctional properties, such as stretchability, self-healing, transparency, tunable hydrophilicity/hydrophobicity, and flame retardancy, attracting extensive research interest [4–7]. Currently, the reported PICs primarily include polymer gels (e.g., hydrogels, ionogel, organogels) and all-solid-state polymer ionic conductors. In polymer gels, a polymer scaffold provides mechanical elasticity, while ions dissolved in a liquid phase (e.g., aqueous solution, organic solution,

or ionic liquid) migrate freely through the polymer network to enable conductivity. Solid PICs are typically formed by complexing polar polymers containing heteroatoms (such as O, S, Si, N) with metal salts. The metal salt ions (e.g., Li^+) can dynamically coordinate and dissociate with lone pair electrons of the heteroatoms on the polymer chains. Through the motion of the molecular chains, long-range transport of metal ions along and between the polymer chains is ultimately achieved. However, a critical scientific challenge persists: the inherent trade-off between mechanical and electrical properties in PICs. Decoupling this relationship to synergistically enhance both performance and aspects is essential for their advancement. Furthermore, in the context of sustainable development and the demand for environmentally friendly materials, the preparation of high-performance PIC with multiple desirable properties from renewable resources has become a major focus in scientific research [8–14].

This urgency has driven the development of composite PIC materials that integrate multiple functionalities such as being cost-effectiveness, environmental friendliness, strong mechanical properties, high electrical conductivity, and excellent biocompatibility [15,16]. Cellulose, the most abundant natural polymer on Earth, emerges as an ideal candidate. It is not only renewable and biodegradable but also exhibits excellent biocompatibility, and its surface is rich with hydroxyl and other tunable functional groups. By establishing intermolecular hydrogen bonds within cellulose chains or using cross-linking agents to form covalent bonds with cellulose molecular chains, cellulose can combine or cross-link with PICs to form a three-dimensional cellulose network [5], resulting in what is termed Cellulose Composite Polymer Ionic Conductors (CPICs). These CPICs exhibit superior physical and chemical properties, including high flexibility, excellent mechanical strength, and enhanced conductivity, thereby significantly broadening their application scope and meeting the demands of numerous fields.

This review systematically examines the preparation and applications of various CPICs, including cellulose composite hydrogels, cellulose composite ionogels, and cellulose composite all-solid-state polymer ionic conductors. Focusing on recent advances, we present optimization strategies for improving mechanical properties, electrical conductivity, environmental stability, and strain-sensing performance (Figure 1). Finally, we summarize the current challenges and future prospects for CPICs, aiming to accelerate the development and practical applications of multifunctional electronics and embodied intelligence.

Figure 1. Classification, application areas, crosslinking strategies, and key properties of cellulose-composite polymer ionic conductors.

2. Classification of CPIC

2.1. Cellulose Composite Hydrogels

Hydrogels are gel materials characterized by their high water content and three-dimensional network structure. They have been extensively studied for their tunable physical, chemical, and biological properties, as well as its high biocompatibility and versatile fabrication methods [17]. However, conventional hydrogels often suffer from limitations such as limited stretchability, poor stability, and insufficient stimulus responsiveness, which restrict their practical applications [8].

In response to growing environmental concerns, hydrogels derived from natural polymers have garnered significant attention. Their advantages include wide resource availability, sustainability, biodegradability, biocompatibility, low cytotoxicity, and cost-effectiveness. Cellulose solution, in particular, has emerged as a promising base material due to its exceptional capacity to absorb electrolytes while maintaining structural integrity. Through chemical and physical cross-linking strategies, cellulose can be modified to enhance key properties, such as hydrophilicity, mechanical strength, environmental stability, and biocompatibility. Hydroxyl groups are on the cellulose polymer to facilitate hydrogen bonding and serve as active sites for chemical modification [18]. This enables the creation of functionalized structures that not only enrich the functionality of cellulose but also promote the formation of cross-linked networks, leading to versatile cellulose composite hydrogels (CCHs) with tailored properties.

CCHs hold broad application prospects in wearable electronics, agriculture, and biomedical care [19–21]. A significant limitation, however, is their operational temperature range; the aqueous phase freezes at temperatures below 0 °C and evaporates rapidly at elevated temperatures, severely degrading electrical conductivity, mechanical properties, and transparency. Furthermore, the addition of conductive fillers can compromise both the mechanical stability and electrical performance of CCHs [8,22]. Current research is therefore focused on novel modification techniques and eco-friendly additives to enhance the stability and environmental adaptability of CCHs without sacrificing their biocompatibility and functionality.

2.2. Cellulose Composite Ionic Gel

Ionic gels (or ionogels) primarily consist of a polymer network infused with an ionic liquid (IL), which is an organic molten salt composed solely of cations and anions. Although a liquid phase is present, the cross-linked polymer network immobilizes it, preventing flow. This structure disrupts the ordered arrangement of polymer chains, thereby optimizing ion transport efficiency while maintaining excellent structural stability [23]. Compared to hydrogels, ionic gels offer superior properties, including freeze resistance, low volatility, flame retardancy, high ionic conductivity, and thermal stability [7,24,25]. However, their polymer networks are typically synthesized from non-degradable petroleum resources [26].

Following a rationale similar to that for cellulose hydrogel, cellulose can serve as a sustainable three-dimensional polymer network to form cellulose composite ionic gels (CCIGs). The cellulose matrix contributes to effective adsorption and storage of ILs, facilitating their uniform distribution. CCIGs exhibit numerous advantages, such as high transparency, low volatility, excellent thermal and chemical stability, freeze resistance, high ionic conductivity, and antibacterial properties. Their recyclability via simple thermal treatment—while retaining most original electrical performance—further underscores their environmentally friendly nature. The combination of these properties makes CCIGs highly promising for a wide range of applications, such as flexible electronic devices, sensors, and environmental monitoring [27–30].

Despite its broad application potential due to excellent ionic conductivity, CCIGs faces challenges as the high concentration of IL may compromise its mechanical strength and pose potential leakage risks. IL leakage not only reduces the material's conductivity but may also pose environmental and health hazards. Furthermore, the long-term stability and sensitivity of CCIGs as a sensing material often fall short of ideal performance in practical applications. Microscopically, polymer chains within the gel may undergo rupture due to excessive or cyclic local stress, and microcracks may initiate and propagate over time, potentially degrading the overall material performance. Thus, when considering the structural reliability of gel materials in practical use, macroscopically, inhomogeneities within the gel material—such as pores, impurities, or localized structural inconsistencies—can lead to stress concentration and accelerate material fatigue, which may further compromise the material's long-term mechanical stability (e.g., resistance to stretching or compression) and service life in applications like flexible strain sensors or wearable electronic components [31].

Consequently, developing conductive materials that simultaneously offer high mechanical stability, efficient ion transport, superior fatigue resistance, insensitivity to crack propagation, and high sensitivity is crucial to meet the rapidly growing demands in various fields such as flexible skin-like electronics, energy storage, and wearable devices.

2.3. Cellulose Ion-Conducting Elastomer

Ion-conducting elastomers (ICEs) are composed of a polymer host and alkali metal salts. Cations achieve charge transport by "hopping" between polar or Lewis acid-base active groups (e.g., $-C=O-$, $-C-O-$, $-P-$, $-N-$, $-S-$, and $-C=N-$) via dynamic bonds formed by the reaction of alkali metal salts with these functional groups [32–34]. Currently, the room-temperature ionic conductivity of ICEs typically ranges from 10^{-4} to 10^{-2} mS/cm, which falls far short of the requirement for most flexible electronic devices (>1 mS/cm) [34].

Cellulose offers polar functional groups (such as hydroxyl, carboxyl, or ether groups), which can effectively complex with Li^+ to enhance ion migration and improve the overall ion-conducting performance of the elastomer. The incorporation of cellulose, particularly after physical or chemical treatment weakens the intermolecular interactions by disrupting hydrogen-bonding networks [35], introducing steric hindrance [36], or reducing crystallinity [37] within cellulose and improves the material's toughness, resulting in flexible molecular chains with a greater number of polar groups [38]. Through treatments such as blending [39], copolymerization [40], or cross-linking [41], cellulose composite solid polymer ionic conductors, referred to as cellulose ion-conducting elastomer (CICEs), can be synthesized. These materials represent a highly promising class of polymer electrolytes, combining the sustainability of cellulose with enhanced ionic conductivity and mechanical flexibility [42].

3. Optimization of Mechanical Properties

For emerging applications of flexible and stretchable electronic devices, the exceptional mechanical characteristics and outstanding fatigue resistance of CPICs are critical to ensuring their reliability and prolonged service life. This section will explore and summarize effective strategies for enhancing the mechanical and fatigue performance of CPIC materials.

3.1. Enhancement of Mechanical Strength

The polymer matrix serves as the primary mechanical framework in CPICs. Strategies for improving mechanical performance focus on the following two aspects: (1) optimizing the

cross-linked network structure of the polymer matrix, and (2) enhancing the interfacial interaction between the conductive component and the polymer network. Specific reinforcement approaches include physical/chemical cross-linking [22,43–45], polymer blending [4,46–49], hybrid reinforcement [43,50,51], incorporation of dopants and plasticizers (e.g., clay, carbon nanotubes, TiO_2, Fe_3O_4, and nanoparticles) [52–54], and graft copolymerization [46].

The use of physical or chemical cross-linking to form dual or multiple network structures through hydrogen bonds, covalent bonds, and ionic bonds can significantly enhance both the strength and toughness of the material. For instance, Huang et al. [55] utilized a hybrid physical network of nanocellulose/Fe^{3+}/polyacrylamide (PAM) cross-linked with a flexible chemical network to fabricate a CCH with exceptional stretchability. The resulting material exhibited a tensile stress of 128.6 kPa and an elongation of 2795% (Figure 2a). Zhao et al. [44] dissolved cellulose in an alkali/urea/water system and constructed a dual-network structure through continuous chemical cross-linking with epichlorohydrin (ECH) combined with ethanol-induced physical cross-linking. This approach successfully yielded a mechanically strong and tough CCH, exhibiting a maximum tensile strength of 2.7 MPa, a fracture elongation of 81%, and a fracture energy of 0.85 MJ/m^3 (Figure 2b). Similarly, Shu et al. [56] dissolved cellulose (cotton linter) using $ZnCl_2$/$CaCl_2$ and designed and prepared a dually cross-linked CCH via ECH. By optimizing the cross-linking density and adjusting the ECH content, they successfully fabricated a CCH with a tensile strength of 0.82 MPa and a fracture elongation of 260%. These results demonstrate that this method leads to significant improvements in fracture stress, higher deformation capability, and enhanced energy dissipation. The combination of chemical and physical dual cross-linking offers a novel strategy for constructing high-strength cellulose hydrogels.

Self-healing properties refer to the ability of a material to autonomously restore its structural integrity, mechanical performance, or functionalities (such as ionic conductivity and elasticity) after suffering physical damage (e.g., microcracks, scratches, or partial fractures) through intrinsic repair mechanisms such as dynamic bond reorganization, molecular chain migration, and component diffusion. Cheng et al. [57] designed a CCH featuring a dual cross-linked network composed of dialdehyde cellulose nanofibrils (DCNF), adipic dihydrazide-modified sodium alginate (SA-ADH), polyvinyl alcohol (PVA), and borax. The incorporation of DCNF significantly enhanced the tensile properties of the CCH, achieving a tensile strain of up to 1440%. The DCNF-CCH exhibited excellent self-healing efficiency of tensile strength (>92%), calculated as the ratio of tensile strain at the breaking point of the healed gel over the initial tensile strain of the original sample, within 60 min without any external stimulus (Figure 2c). Zhang et al. [58] utilized an epoxide ring-opening reaction to convert the secondary hydroxyl groups in the heterogeneous structure of cellulose into primary hydroxyl groups, significantly enhancing the flexibility of molecular chains and the formation of dynamic hydrogen bonds. Benefiting from its unique physically cross-linked network structure and non-Newtonian behavior, the resulting CCH exhibited an extraordinary maximum tensile strain of 44,200%, a tensile strength as high as 226 MPa, and maintained a high Young's modulus of $9.4 \pm 1.1 \times 10^3$ MPa at 3.5% strain, along with rapid self-healing properties (Figure 2d). This performance successfully surpasses that of existing all-cellulose hydrogel materials, not only advancing the development of ultra-stretchable all-cellulose hydrogels but also opening new possibilities for applications in wearable devices.
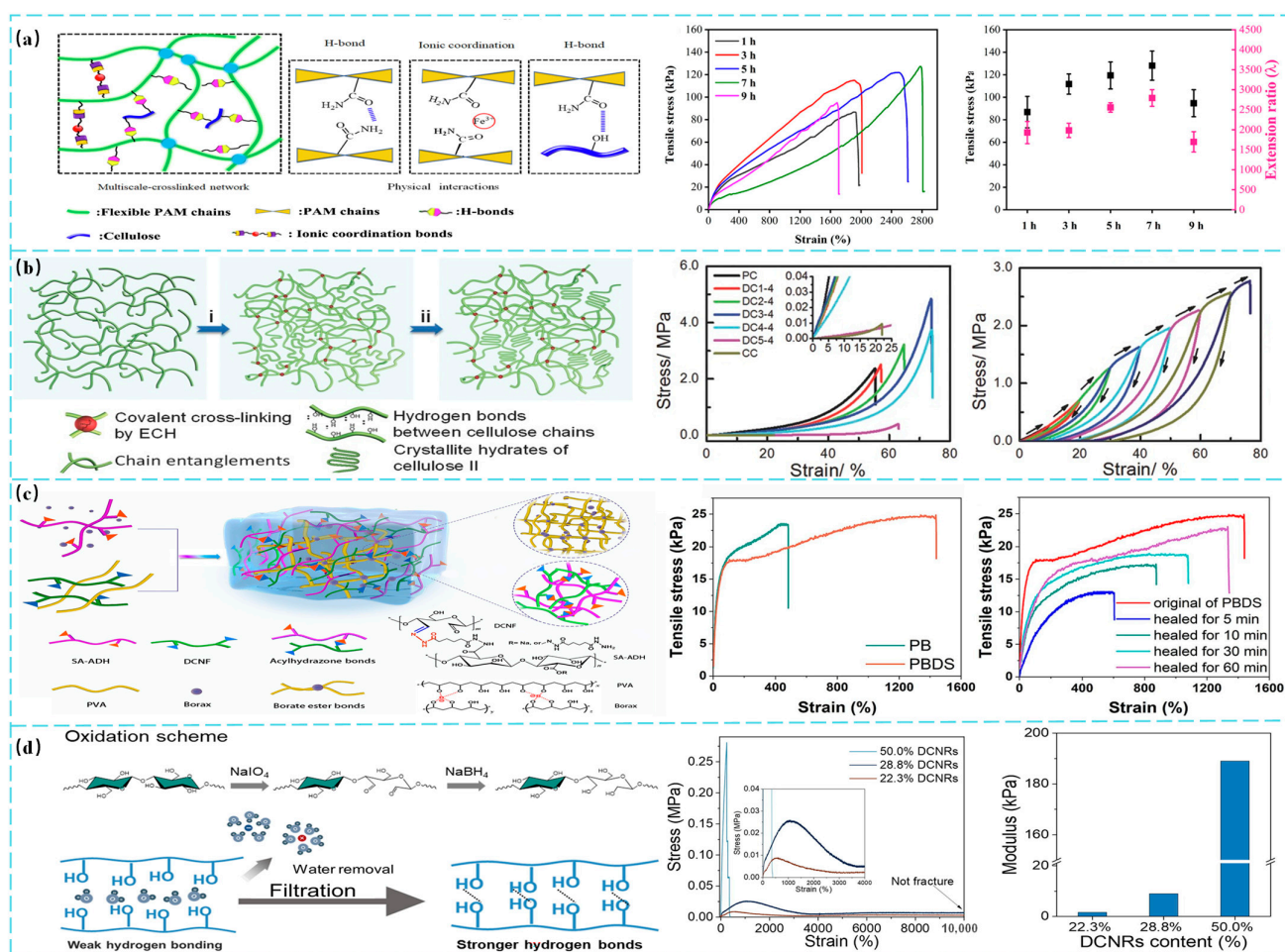
Figure 2. Investigating the mechanical properties of CCHs. (**a**) Structure, tensile stress–strain curves, corresponding tensile stress, and extension ratio of PAM/Fe^{3+}-CCH under different ball milling times (Reprinted with permission from [55]). (**b**) Structure, compressive stress–strain curves of physically cross-linked cellulose hydrogel (PC), CCH with varying molar ratios of ECH, and chemically cross-linked cellulose hydrogel (CC) under compression (Reprinted with permission from [44]). (**c**) Schematic illustration, strain–stress curves of CCH before and after the incorporation of DCNF, strain–stress curves after self-healing for 5, 10, 30, and 60 min and various maximum stretching (Reprinted with permission from [57]). (**d**) Fabrication process, stress–strain curves and the corresponding modulus of CCH with varying contents of dialdehyde cellulose nanorods (DCNR) (Reprinted with permission from [58]).

The key mechanism in CCIG involves the incorporation of weak or dynamic bonds—existing either directly between polymer chains or mediated by ionic liquids—as sacrificial bonds within the network. These bonds effectively dissipate energy during material deformation, thereby enhancing toughness [59].

Inspired by natural rubber, Qian et al. [60] substituted the hydroxyl groups on the D-glucose units of cellulose with cyanoethyl groups, transforming the cellulose molecules into a coiled conformational design. This approach led to the synthesis of an ionogel with ultra-stretchability, exhibiting a tensile strength of up to 1.8 MPa and a maximum tensile strain of nearly 1000% (Figure 3a). Jiang et al. [61] redesigned and reconstituted cellulose molecules by leveraging the distinct hydrogen bonding and electrostatic interactions between 1-butyl and 3-methylimidazolium chloride ([Bmim]Cl) and 1-ethyl-3-methylimidazolium tetrafluoroborate ([Emim]BF_4). By strengthening the hydrogen bond network within cellulose while weakening the electrostatic interactions in the cellulose framework, they successfully fabricated a CCIG with a tensile strength of 3.5 MPa, capable of lifting weights

exceeding 1428 times its own mass (Figure 3b). Guo et al. [62] dissolved cellulose using 1-ethyl-3-methylimidazolium acetate ionic liquid ([EMIM][OAc]) and performed in situ cross-linking via a ring-opening reaction between bisphenol epoxy resin and ceric ammonium nitrate. With halloysite nanotubes (HNTs) incorporated as an ion-conducting promoter, a high-performance CCIG was successfully fabricated. The mechanical properties were significantly enhanced, exhibiting an elastic modulus of 6.1 MPa, a tensile strength of 3.2 MPa, and an elongation at break of 70.1%. Moreover, the modulus remained stable even at high temperatures up to 200 °C (Figure 3c). Chen et al. [63] introduced carboxymethyl cellulose (CMC) into a polyacrylic acid (PAA)/Fe^{3+} hydrogel system. By leveraging the synergistic interaction between the physical ionic network of $-COO^-$/Fe^{3+} and the covalent network of PAA, a high-density network was formed. Subsequent immersion in a NaCl solution introduced sacrificial bonds (or weak bonds) for energy dissipation. The resulting material exhibited a tensile strength of 4.42 MPa, an elongation at break as high as 750%.

In solid-state ionic conductors, cellulose is commonly employed as a mechanical reinforcement material [64]. It is frequently used as a supporting substrate in solid electrolyte membranes, enabling them to withstand stresses encountered during battery encapsulation processes. Furthermore, cellulose effectively inhibits the formation and growth of dendrites during the plating of alkali metal anodes [65]. Zhao et al. [66] utilized low-cost and widely available cattail fibers to fabricate a CICE for lithium-ion batteries (LIBs) through 2,2,6,6-tetramethylpiperidine-1-oxyl (TEMPO) oxidation and vacuum filtration. The resulting material exhibited excellent thermal dimensional stability, high tensile strength (75 MPa). Deng et al. [67] added cellulose acetate (CA) and polyurethane (PU) to a UIO-67 (a metal–organic framework, MOF) solution and fabricated a CA/PU–MOF separator via electrospinning. Polyurethane was employed to facilitate the formation of a uniform nanoporous structure within the cellulose acetate framework, thereby enhancing mechanical properties. The results demonstrated that the CA/PU–MOF separator exhibited increases of 620% in elongation at break and 28.4% in tensile strength (Figure 3d). Wang et al. [68] achieved nanofibrillation and chemical modification of cellulose in deep eutectic solvent (DES) systems composed of lactic acid/choline chloride (LA/ChCl) or maleic acid/choline chloride (MA/ChCl). Using a straightforward one-pot method or 3D printing, they fabricated physically and chemically cross-linked cellulose nanofibril (CNF) /PDES conductive elastomers. The addition of varying CNF contents increased the stress of the elastomer by 6 to 8 times (Figure 3e). Similarly, Ning et al. [13] employed an ultraviolet (UV)-initiated in situ polymerization method to integrate a polymerizable deep eutectic solvent (PDES), synthesized from protic acid/choline chloride (PA/ChCl), with a CNF aerogel. Phytic acid was introduced to enhance the binding interaction between CNF and PDES, resulting in an ionically conductive elastomer rich in both covalent and non-covalent (hydrogen) bonds. The obtained material achieved a stress of 0.38 MPa and a strain of 1378% (Figure 3f).

Enhancing the mechanical properties in CPICs primarily relies on optimizing the polymer cross-linked network and strengthening the interaction between the conductive component and the polymer host network [69]. Strategies such as physical and chemical cross-linking are not only highly effective but also feature straightforward synthesis processes, making them the most widely applied approaches. CPICs improve mechanical performance by reinforcing the entanglement and interpenetrating network structure between polymers and cellulose fibers. Key approaches include chemically modifying active sites on cellulose into effective derivatives, regulating polymer conformation via pH, temperature, and solvent effects, and introducing highly polar and long-chain polymers containing heteroaromatic rings to increase cross-linking density and dynamic interactions [70,71].
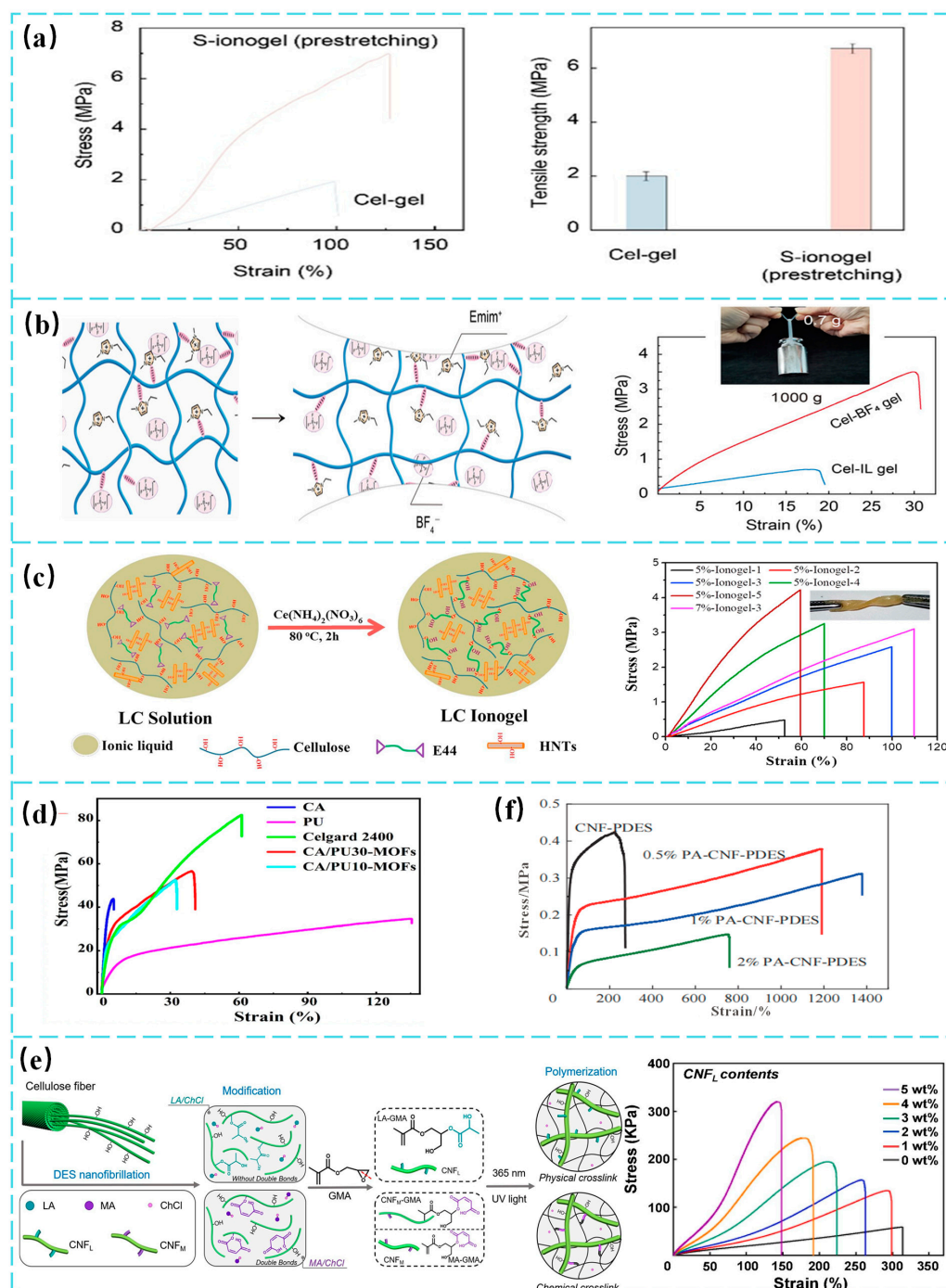
Figure 3. Investigating the mechanical properties of CCIGs and CICEs. (**a**) Tensile stress–strain curves and tensile strength comparison of S-ionogel (pre-stretched to 80% strain) and Cel-gel (Reprinted with permission from [60]). (**b**) Schematic illustration demonstrating the robust mechanical properties of Cel-BF$_4$ gel and the tensile stress–strain curves of Cel-BF$_4$ gel and Cel-IL gel (Reprinted with permission from [61]). (**c**) Stress–strain curves of CCIG with varying cellulose and HNTs contents (Reprinted with permission from [62]). (**d**) Stress-stain curves of CA/PU-MOF diaphragm prepared by electrostatic spinning (Reprinted with permission from [67]). (**e**) Fabrication process, tensile stress–strain curves of LA/PDES conductive elastomers with varying CNF contents (Reprinted with permission from [68]). (**f**) CICE with varying CNF/PDES content (Reprinted with permission from [13]).

3.2. Enhancement of Fatigue Resistance

In practical applications for conductive sensing capabilities, CPICs should possess not only high strength and good ductility but also considerable fatigue resistance and excellent

resilience to ensure accurate signal transmission during repeated deformation. Enhancing the fatigue resistance of CPICs is therefore essential to improve their mechanical stability and long-term durability.

The dual-network structure fabricated by Zhao et al. [44] through continuous chemical cross-linking and ethanol-induced physical cross-linking enables the cellulose network to fully recover its compressive stress to the original state after each unloading cycle at 70% strain, exhibiting significant hysteresis and relatively minor permanent deformation (Figure 4a). Similarly, Lian et al. [72] employed a dual-network architecture based on hydrogen bonding interactions between cellulose and PVA, reinforced by Zn^{2+} coordination with hydroxyl groups of cellulose. In the optimized sample with 5 wt% PVA content (Gel-5), no significant loss in ultimate stress was observed after 50 compression cycles at 50% strain (Figure 4b).
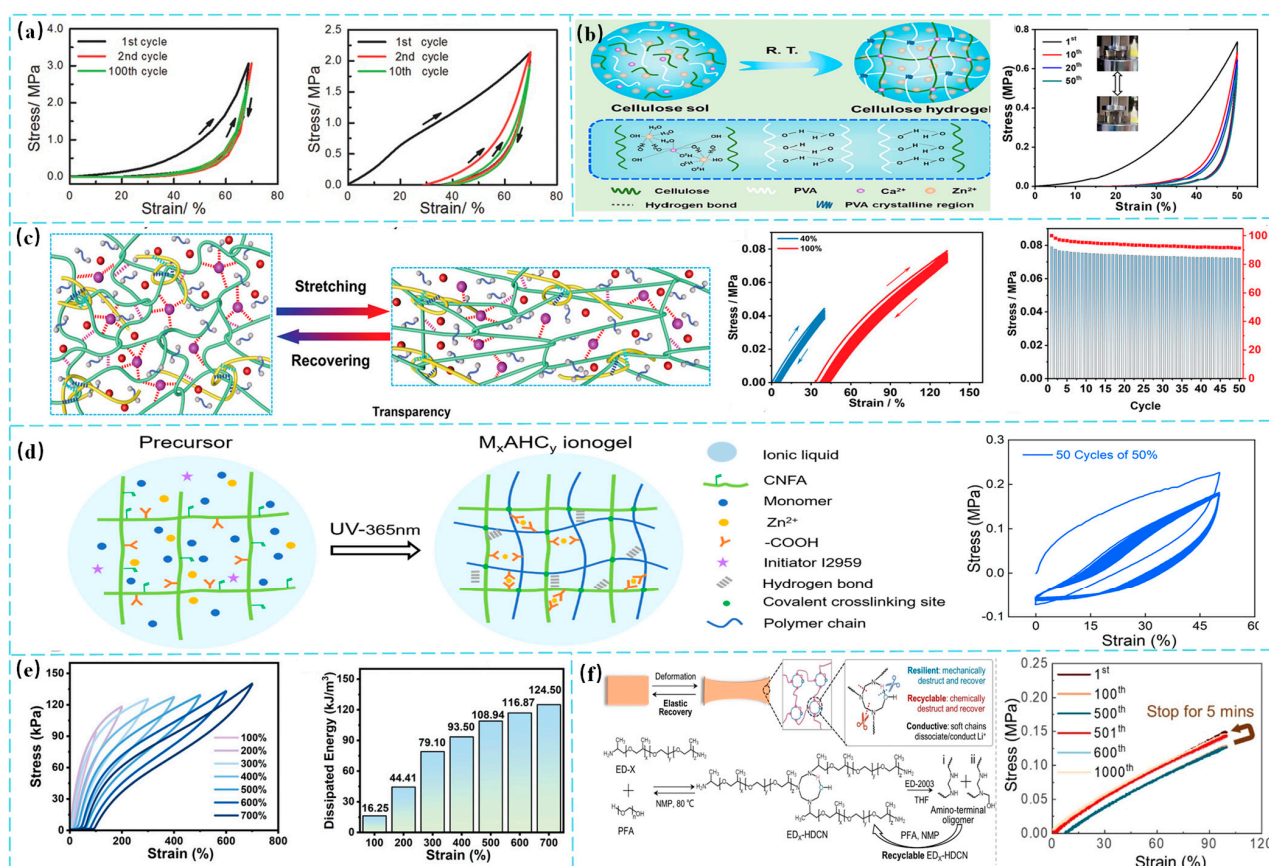

Figure 4. Investigating the fatigue resistance of CPICs. (**a**) Tensile stress–strain curves of DC3-4 under loading–unloading cycles at 70% strain for the 1st, 2nd, and 100th cycles (Reprinted with permission from [44]). (**b**) Schematic illustration Preparation, cyclic compressive stress–strain curves of Gel-5 over 50 consecutive cycles (Reprinted with permission from [72]). (**c**) Schematic illustration of the high resilience mechanism, continuous loading–unloading curves of $ZnCl_2/EG_4/AA_2/HPC_1$ at 40% and 100% strain, and the mechanical strength retention rate after 50 loading–unloading cycles at 100% strain (Reprinted with permission from [6]). (**d**) Schematic preparation, tensile loading–unloading curves of MAHC ionogel at 50% strain over 50 consecutive tensile cycles (Reprinted with permission from [73]). (**e**) Tensile loading–unloading curves of AC_2TC_2 at different strains and the corresponding dissipated energy (Reprinted with permission from [74]). (**f**) Illustration of the reversible stress dissipation provided, stress–strain curves of ED over 1000 cycles at a fixed strain of 100% under tensile conditions (Reprinted with permission from [75]).

Lu et al. [6] introduced hydroxypropyl cellulose (HPC) into a metal salt-based deep eutectic solvent (MDES) and fabricated a CCIG via in situ photopolymerization. This gel

combines permanently entangled PAA polymer chains and dense dynamic bonds capable of rapid breaking/reconstruction, resulting in a mechanical strength retention rate of up to 91.4% after 50 loading-unloading cycles, along with high elasticity (exhibiting 98.1% recovery) (Figure 4c). Li et al. [73] fabricated a CCIG using allyl glycidyl ether-modified nanocellulose (CNFA) and Zn^{2+} as a macromolecular covalent cross-linker and a dynamic metal-ion cross-linker, respectively. The modified CNFA provided multiple reactive sites for chemical cross-linking with polymer chains of varying lengths. The material was tested over 50 cycles at 50% strain, retaining 80% of its initial tensile stress. The first loading–unloading curve exhibited a significant hysteresis loop with high energy dissipation, while subsequent cycles remained stable and nearly overlapping, confirming a resilient and recoverable elastic network (Figure 4d).

Zhang et al. [74] incorporated tannic acid-encapsulated cellulose nanocrystals (TA@CNC) as multifunctional hydrogen bond donors (HBD) into a system with poly-acrylic acid (PAA) and choline chloride (acting as hydrogen bond acceptor, HBA), forming a dynamically cross-linked network through multiple dynamic hydrogen bonds. Continuous cyclic tensile loading–unloading tests were conducted on the resulting CICE at strains increasing from 100% to 700%. The material exhibited significant hysteresis loops, and the energy dissipated per unit volume increased progressively from 16.25 kJ/m^3 to 124.50 kJ/m^3 (Figure 4e). Yin et al. [75] constructed a dual dynamic cross-linked network utilizing hemiaminal dynamic covalent bonds (HDCN) combined with soft copolymer chains containing $-O-CH_2-CH(CH_3)-$ and $-O-CH_2-CH_2-$ segments. The hemiaminal cross-linking points feature weak intramolecular hydrogen bonds and relatively strong $-C-N-$ bonds. After 1000 cycles, the hysteresis ratio was only 2.03%. The loading–unloading curves at various strains showed no hysteresis loops, and the strength remained nearly constant throughout the 1000 cycles (Figure 4f).

Overall, the most effective strategy for optimizing the performance of conductive polymer ionic conductors (CPICs) is to construct a dual-network architecture comprising a permanent backbone and reversible sacrificial bonds—using hydrogen bonds, metal–coordination bonds, or dynamic covalent bonds as multifunctional crosslinking sites to provide energy dissipation and rapid recovery, thereby improving load transfer and durability; [59]. These strategies collectively enhance both the toughness and fatigue resistance of CPIC. However, optimizing fatigue resistance must be balanced with the preservation of electrical properties, mechanical strength, and recyclability. Future research should focus on identifying optimal trade-offs among multiple performance metrics to facilitate the broad applications of CPICs across flexible electronics, sensing, and energy devices.

4. Optimization of Electrical Conductivity

The electrical conductivity of CPICs is a critical factor for their applications in flexible and stretchable electronic devices and electrochemical systems. Both the polymer matrix and added functional materials influence conductivity, which not only determines the operational efficiency and stability of electronic devices but also directly affects the energy conversion efficiency and response speed of electrochemical devices. Due to the inherent coupling between mechanical and electrical properties, the conductivity primarily relies on the concentration and mobility of mobile ions within the system. Thus, the principal strategies for enhancing CPIC conductivity involve increasing ion concentration and improving ion mobility [9].

In CCHs, the ionic conductivity at room temperature typically ranges from 0.1 to 1 mS/cm. A common method to enhance conductivity is the incorporation of conductive substances such as salts [17], which form a three-dimensional network within the polymer matrix through physical or chemical cross-linking. The addition of metal salts like $ZnCl_2$,

CaCl$_2$, AlCl$_3$, and FeCl$_3$ not only increases ion concentration but also improves the freeze resistance of CCHs. Freeze resistance refers to the ability of a material to maintain its structural integrity and electrical and mechanical properties under low temperature or freeze–thaw cycling conditions. Upon dissolution, metal salts dissociate into cations and anions, which interact strongly with free water molecules or polar groups within the system—such as hydroxyl or amino groups in polymer matrices—through mechanisms including ion-dipole interactions and hydrogen bonding [76]. These interactions significantly lower the freezing point of the system, thereby preventing water from crystallizing at low temperatures. The inhibition of ice crystal formation avoids damage to ion transport pathways while preserving mechanical flexibility and structural integrity. For instance, introducing ZnCl$_2$/CaCl$_2$ into the cellulose dissolution system [56,77] enables Zn^{2+} ions to coordinate with hydroxyl groups on cellulose chains, facilitating cellulose dissolution, while Ca^{2+} ions act as cross-linkers through ionic interactions and hydrogen bonding, serving as gelling agents. This approach not only inhibits ice crystallization within the hydrogel but also endows CCH with high ionic conductivity and excellent mechanical properties. The ionic conductivity of CCH can also be enhanced by incorporating polymers such as polyacrylamide (PAM) [78], epichlorohydrin (ECH) [56], polyacrylic acid (PAA) [79], bentonite (BT) [79,80], and benzyltrimethylammonium hydroxide (BzMe$_3$NOH) [81]. These additives form dual-network structures with cellulose, strengthening the interaction between the polymer matrix and conductive components, thereby improving both electrical conductivity and mechanical properties. Additionally, modifying cellulose to introduce specific functional groups that form covalent bonds with polymers represents an effective strategy for further enhancing the material's conductivity. Chen et al. [82] grafted a copolymer of acrylonitrile (AN) and acrylamide (AM) onto hydroxypropyl methyl cellulose (HPMC) chains to obtain a CCH with a conductivity of up to 15.4 mS/cm. The resulting material exhibits excellent electrical and mechanical properties, demonstrating significant potential for applications in wearable strain sensors.

In CCIGs, ionic liquids possess the ability to dissolve cellulose and can serve as reaction media for producing functional cellulose derivatives. The strong interactions between ionic liquids and cellulose polymer backbone facilitate the construction of a continuous and dense conductive network [12], thereby significantly enhancing the electrical conductivity of the material. Taking 1-butyl-3-methylimidazolium chloride ([BMIM]Cl) as an example, it is recognized as one of the most suitable ionic liquids for dissolving and processing cellulose. It enables in situ splitting (nanofibrillation) and molecularization of cellulose fibers within the ionic liquid matrix, forming multi-scale or tunable hydrogen-bonded systems or topological structures. This enhances the physicochemical properties of CCIG while effectively increasing ion mobility through hydrogen bonding guidance. Consequently, the electrical and mechanical performance of the gel material (See the first sentence of Section 2.1) is substantially improved without the need for increasing ion concentration [60,83,84].

However, its limitation lies in its high viscosity, which slows down the dissolution rate of cellulose. This issue is commonly addressed by using low-viscosity ionic liquids as solvents or incorporating cosolvents such as dimethyl sulfoxide (DMSO) or acrylamide (AM) [12]. In this context, Li et al. designed a polymerizable deep eutectic solvent (PDES) composed of [BMIM]Cl and AM and introduced cellulose into the PDES system to construct a high-performance and multifunctional CCIG. The addition of AM reduced the viscosity of [BMIM]Cl, promoted ion dissociation, and achieved a high ionic conductivity of 24.4 mS/cm. Additionally, ion concentration is positively correlated with ionic conductivity, but this relationship holds only within a certain concentration range. When the salt concentration exceeds the solvation capacity of the solvent, aggregation of cations and anions occurs—leading to the formation of larger ion clusters—which in turn reduces the number of freely mobile ions in the solution, thereby adversely affecting the conductivity [85,86].

In CICEs, ion transport primarily occurs in the amorphous regions of the polymer, while high crystallinity restricts the motion of polymer chains, resulting in low ionic conductivity (typically 10^{-4} to 10^{-2} mS/cm at room temperature), which fails to meet the requirements for flexible electronics. Therefore, one of the key strategies to enhance the ionic conductivity of CICEs is to reduce the crystallinity of the polymer. This can be achieved through methods such as blending or copolymerization [87,88], cross-linking [89,90], incorporation of inorganic fillers [91,92], and addition of small-molecule plasticizers [14,93]. The summary of the conductivity under optimized strategy for CPIC is shown in Table 1.

Table 1. Conductivity under optimized strategy for CPIC.

CPIC	Material	Salt Medium	Conductivity (mS/cm)	Reference
CCH	Cellulose	$ZnCl_2/CaCl_2$	749	[77]
	Cellulose + ECH	$ZnCl_2/CaCl_2$	548	[56]
	Cellulose + PAM	$AlCl_3/ZnCl_2$	270	[94]
	Cellulose + PAA + BT	$ZnCl_2$	88.9	[79]
	Cellulose + BT	LiCl	89.9	[80]
	Cellulose + BzMe$_3$NOH	NOH	237	[81]
	Cellulose + PDA + PAM	FeCI$_3$	240	[78]
	HPMC + AN + AM	$ZnCI_2$	154	[82]
CCIG	Cellulose + AM	[Bmim]Cl	244	[95]
	HPC + LA + AA	[C2VIm]Br	3.29	[31]
	Cellulose	[Emim]OAc	59.5 ± 4.7	[96]
	Cellulose	[Bmim]Cl	40	[84]
	Cellulose + silk fibers	[Bmim]Cl	49.6	[83]
	Cyanate Cellulose	[Bmim]Cl	21.35	[60]
CICEs	CLA + LATP		1.1	[35]
	CP	[Amim]Cl	1.09	[97]
	Cellulose + TEMPO		2.83	[66]
	HEC + NMA	LiTFSI	1.61	[98]
	CLA + LATP	LiTFSI	1.25	[99]

Footer: ECH: Epichlorohydrin; PAM: Polyacrylamide; PAA: Poly(acrylic acid); BT: Bentonite; BzMe$_3$NOH: Benzyltrimethylammonium hydroxide; PDA: Polydopamine; HPMC: Hydroxypropyl methylcellulose; AN: Acrylonitrile; AM: Acrylamide; LA: Lactic acid; AA: Acrylic acid; [Bmim]Cl: 1-Butyl-3-methylimidazolium chloride; [Emim]OAc: 1-Ethyl-3-methylimidazolium acetate; CLA: Cross-linked cellulose; LATP: Lithium aluminum titanium phosphate; CP: Cellulose phosphate; [Amim]Cl: 1-Allyl-3-methylimidazolium chloride; TEMPO: 2,2,6,6-Tetramethylpiperidine-1-oxyl; HEC: Hydroxyethyl cellulose; NMA: N-Methylacrylamide; LiTFSI: Lithium bis(trifluoromethanesulfonyl)imide.

5. Optimization of Environmental Stability

Hydrogel materials use water as the dispersion medium, making them susceptible to freezing below 0 °C and rapid evaporation above 100 °C. Both conditions can cause loss of deformability, restricted ion transport, and severe degradation of performance. To address these issues, researchers often focus on enhancing the freeze resistance of hydrogels, commonly by incorporating organic cryoprotectants (typically polyols such as glycerol and ethylene glycol) or ionic liquids into the medium.

Zhang et al. [77] integrated $ZnCl_2/CaCl_2$ into CCH to improve freeze resistance. Viscoelastic tests showed that the storage modulus and loss modulus of the hydrogel remained stable at temperatures as low as −60 °C, indicating maintained mechanical performance. The addition of glycerol into this mixture further enhanced freeze resistance, allowing the CCH to remain stable down to −100 °C. Wang et al. [100] dissolved cellulose and poly(vinyl alcohol) (PVA) in an aqueous solution of benzyltrimethylammonium hydroxide (BzMe$_3$NOH) and directly prepared an antifreezing CCH through chemical cross-linking. Experimental results demonstrated that the material retained over 90% transparency and stable mechanical properties within a temperature range of −27.8 to 62.1 °C. This behavior is likely attributed to the strong attraction between cellulose and water molecules, which weakens water–water interactions and thereby inhibits ice crystallization [101].

Yan et al. [79] developed a versatile CCH with high ionic conductivity, high mechanical strength, and broad temperature tolerance by incorporating $ZnCl_2$. The coordination bonds between Zn^{2+} and carboxyl groups of PAA, the binding energy between cellulose and bentonite (BT), BT acts as a multifunctional nanofiller, simultaneously reinforcing the mechanical skeleton, optimizing ion transport, and stabilizing the composite across extreme temperatures. The abundant hydrogen bonds within cellulose and PAA (polyacrylic acid) endowed the CCH with remarkable tensile fracture stress (2.39 MPa), compressive strength (17.85 MPa), high ionic conductivity (88.9 mS/cm), and wide temperature adaptability (retaining 30.3 mS/cm even at −60 °C). Shu et al. [56] optimized the preparation conditions and cross-linking density to develop a dual-network CCH exhibiting high electrical conductivity of 54.8 mS/cm. Owing to the inorganic salt-induced antifreeze properties (withstanding −81.0 °C), the material could operate reliably in extremely cold environments.

For CCIG, the incorporation of ionic liquids significantly broadens the operational temperature range of the material. It not only prevents functional degradation caused by water evaporation or freezing but also enhances the thermal stability of the gel, allowing it to remain stable over a wide temperature range and thereby improving environmental adaptability. Zhao et al. [102] synthesized a polyacrylamide (PAAm)-based CCIG using 1-butyl-3-methylimidazolium chloride ([BMIM]Cl), which maintained excellent impact strength (96.35 $kJ \cdot m^2/g \cdot cm^3$) even under extreme cold conditions at −50 °C. Wang et al. [103] developed a CCIG from natural chitosan and cellulose in an ionic liquid, which exhibited high-temperature stability up to 150 °C, antifreeze performance, and high conductivity (approximately 10^{-1} to 10^2 mS/cm) over a broad temperature range from −50 °C to 120 °C. Wu et al. [96] employed 1-ethyl-3-methylimidazolium acetate ([EMIM]OAc) to dissolve cellulose in delignified wood in situ, mitigating the inhibitory effect of surrounding ions on hydrogen bonding between dissolved cellulose macromolecular chains. This process resulted in complete dissolution of cellulose and the formation of a homogeneous solution. Subsequent removal of the inhibitory influence of the ionic liquid on the hydrogen-bonded network enabled the self-assembly of cellulose chains, yielding a CCIG with multifaceted superior properties. Notably, it demonstrated outstanding freeze resistance, maintaining a relatively high ionic conductivity of 6.4 mS/cm even at −50 °C.

Inspired by cucumber tendrils, Li et al. [104] innovatively designed a coiled structure in which soy protein molecules are entangled around cellulose macromolecular chains. This configuration endowed the CCIG with exceptional tensile strength (>30 MPa), enabling it to withstand temperatures above 85 °C while maintaining a tensile strength exceeding 15 MPa, and demonstrating excellent cold resistance down to −20 °C with tensile strength over 10 MPa. This supramolecular conformational design offers a valuable strategy for developing ionogels that combine high strength with environmental tolerance, overcoming the conventional trade-off between mechanical robustness and adaptive performance. Lian et al. [72] constructed a dual-network system based on hydrogen bonding between cellulose and PVA, along with coordination bonds between Zn^{2+} and hydroxyl groups of cellulose. The effective "water-locking" capability of this polymer network resulted in a CCIG with outstanding low-temperature resistance (as low as −90 °C) and storage stability (up to 30 days).

Polymers commonly used to enhance CICE include PEO (polyethylene oxide), PMA (poly(methyl acrylate)), among others [105]. Among these, PEO has attracted significant attention due to its strong lithium-ion solvation ability and high molecular chain flexibility, enabling the transport of Li^+ and Zn^{2+} through segmental motion. However, as a semi-crystalline polymer, PEO exhibits weak chain dynamics in its crystalline regions, resulting in low ionic conductivity (approximately 10^{-6} S/cm) at room temperature for pure PEO-based ICE, which limits its large-scale application.

Inspired by the lithium-ion transport properties of PEO, Xu et al. [98] successfully constructed a composite solid polymer electrolyte (CCSPE) with a DES mass fraction of up to 90%, based on a deep eutectic solvent (DES) system formed through strong hydrogen-bonding interactions between hydroxyethyl cellulose (HEC) and N-methylacetamide (NMA)/lithium bis(trifluoromethanesulfonyl)imide (LiTFSI). This electrolyte system exhibits three key advantages: (1) high ionic conductivity of 1.61 mS/cm at 25 °C; (2) a broad liquid-phase temperature window from −60 °C to 280 °C; and (3) a stable electrochemical window of up to 4.2 V. The study demonstrated that the intermolecular hydrogen-bonding network between DES and HEC not only effectively modulates the solvation structure of Li$^+$ but also significantly enhances the environmental adaptability of the electrolyte across a wide temperature range by improving interfacial compatibility. Samad et al. [106] developed a novel CICE by combining polyethylene oxide (PEO) with networked cellulose (NC). NC suspension is synthesized by opening the structure of microcrystalline cellulose by acidic hydrolysis using sulphuric acid. The drying characteristics of the NC gel enabled the entrapment of PEO, and the embedded PEO within the NC network functioned as ion-conducting pathways while providing structural integrity and stability at temperatures up to 250 °C. With the addition of 15 wt% NC to PEO, the storage modulus increased by more than an order of magnitude at 70 °C, and the thermomechanical behavior was significantly superior to that of pristine PEO across all temperatures, particularly at 60 °C. The maximum ionic conductivity reached approximately 5×10^{-3} mS/cm at 30 °C and 0.9 mS/cm at 80 °C. The decrease in conductivity upon adding 15 wt% NC was not significant at elevated temperatures. The CICE prepared using this method also exhibited an anodic electrochemical stability of 5 V (vs. Li/Li$^+$), making it suitable for application in lithium batteries. The summary of the feasible temperatures and performance of CPIC under optimization strategy is shown in Table 2.

Table 2. Feasible temperatures and performance of CPIC under optimization strategy.

CPIC	Optimization Method	Feasible Temp. (°C)	Performance	Reference
CCH	ZnCl$_2$/CaCl$_2$ + Glycerol	−70–50	Max. Conductivity: 74.9 mS/cm	[77]
	PVA + BzMe$_3$NOH	−27.8–62.1	Transparency: >90%; Stable mechanical properties; Conductivity: 18 mS/cm at 38 °C	[81]
	ZnCl$_2$ + PAA + BT	−60–60	Conductivity: 30.3 mS/cm at −60 °C; 120.2 mS/cm at 60 °C	[79]
	ZnCl$_2$ + PAA	−70–25	Conductivity: 13.9 mS/cm at 25 °C; 6.2 mS/cm at −70 °C	[77]
CCIG	PAAm	−50	Impact strength: 96.35 kJ·m^2/(g·cm^3)	[96]
	Chitosan + [EMIM]OAc	−50–120	Conductivity: 10^{-1} to 10^2 mS/cm	[103]
	Soy Protein + [Bmim]Cl	−20–85	Tensile strength: >30 MPa at 25 °C; >10 MPa at −20 °C; >15 MPa at 85 °C	[104]
	[EMIM]OAc	−25–50	Conductivity: 11.7 ± 1.1 mS/cm at −25 °C; 6.4 ± 0.7 mS/cm at −50 °C	[96]
CICEs	HEC + DES	60–280	Conductivity: 1.61 mS/cm at 25 °C	[98]
	PEO + NC	30–80	Conductivity: 5×10^{-3} mS/cm at 30 °C; 0.9 mS/cm at 80 °C	[106]

Footer: PVA: Poly(vinyl alcohol); BzMe$_3$NOH: Benzyltrimethylammonium hydroxide; PAA: Poly(acrylic acid); BT: Bentonite; PAAm: Polyacrylamide; [EMIM]OAc: 1-Ethyl-3-methylimidazolium acetate; [Bmim]Cl: 1-Butyl-3-methylimidazolium chloride; HEC: Hydroxyethyl cellulose; DES: Deep eutectic solvent; PEO: Poly(ethylene oxide); NC: Nanocellulose.

6. Optimization of Strain-Sensing Performance

With the advent of the Internet of Things (IoT) era, CPICs have found increasingly broad applications in the field of sensors, particularly in electronic skin, health monitoring, and human–machine interfaces [6,59]. In practical applications, sensitivity, response time, and cycling stability are critical metrics for evaluating strain-sensing performance. The following section will discuss optimization strategies focused on enhancing sensitivity and response time.

Sensitivity evaluates the change in electrical resistance of a material in response to external stimuli and is commonly expressed by the Gauge Factor (GF), which represents the relative change in resistance per unit strain:

$$GF = \frac{R - R_0}{R_0 \varepsilon} \tag{1}$$

where R_0 denotes the resistance at zero strain and R represents the resistance at strain ε.

Response time refers to the duration required for a sensor to convert a physical deformation into a measurable sensing signal. For CPIC-based sensors, the response time under loading is typically measured at 10% strain. Shorter response times are desirable for real-time monitoring applications.

According to Figure 5a, CCHs generally show conductivity decreasing with increasing tensile strength across a broad range (nearly 0 to ~12 MPa), though data dispersion reflects the diversity of CCH designs in balancing stress tolerance and ionic transport. CCIGs mainly demonstrate conductivity reduction with tensile strength in the low-stress regime (≈0–2 MPa), where different CCIG designs tune sensitivity to micro-scale strains. CICEs variants exhibit nonlinear conductivity responses in the low-to-medium stress range (≈0–8 MPa)—conductivity first rises (due to structural optimization during stretching) then drops (due to structural damage at higher stress), with each data point's variation stemming from CICEs' diverse structural modifications. Collectively, the scattered yet trend-driven data across all three categories illustrate how material design (e.g., composition, morphology) modulates the stress-conductivity relationship, enabling tailored strain-sensing behaviors for different application scenarios.
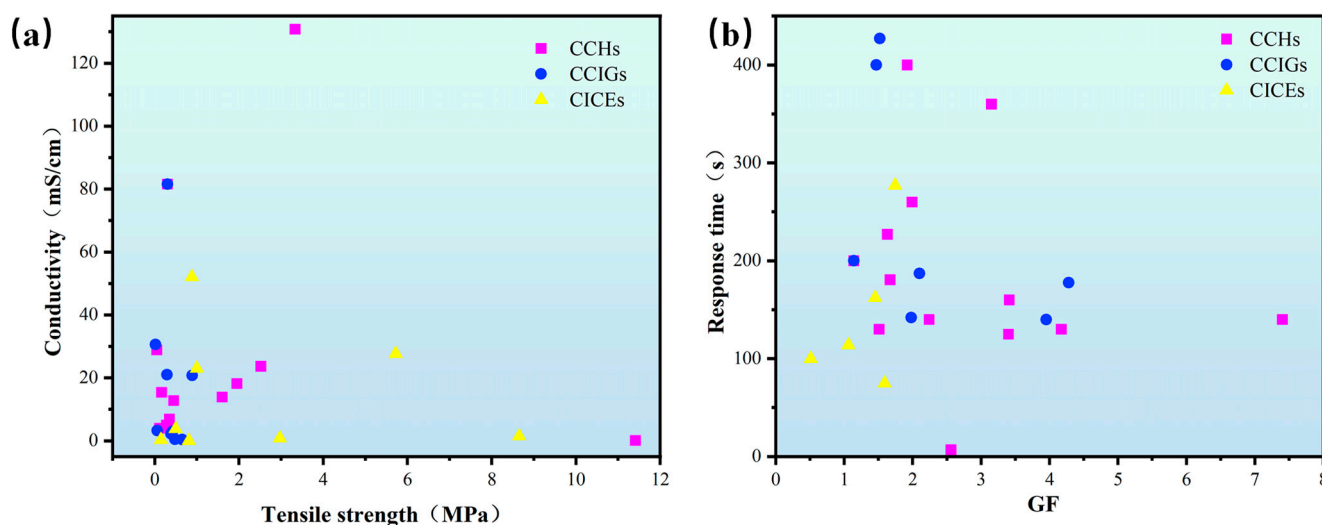

Figure 5. Correlations between key strain-sensing properties of CPICs (**a**) Correlation between electrical conductivity and tensile strength (**b**) Relationship between GF and response time.

According to Figure 5b, CCHs show a wide range of gauge factor (GF:1.5–7.4) and response time (7–400 s), reflecting flexible material design trade-offs between sensitivity and

response speed; CCIGs mainly exhibit GF in 1.1–4.3 with response times of 140–427 s, where higher GF tends to correspond to shorter response times (optimizing speed at moderate sensitivity); and CICEs have relatively lower GF:0.51–1.744 but faster response times (75–277 s), prioritizing rapid strain detection via material design. Overall, differences in composition and structure enable each category to offer tailored strain-sensing performance (sensitivity vs. response timeliness) for diverse applications.

Variations in sensitivity and response time due to strain are closely related to the material's structure and properties, the rate of strain application, and the mechanism of electrical signal transduction [107]. The key strategy for improving both sensitivity and response time lies in ensuring that the conductive pathways within the material undergo significant changes in response to minor deformations. Ideally, CPIC should form a stable conductive network that adheres to the substrate and deforms synchronously with it. The summary of strain-sensing metrics for representative CPIC-based sensors is shown in Table 3.

The microstructure of the material is crucial for regulating sensitivity and response time. Semi-interpenetrating networks (PAAm/CMC), double networks (PVA/borax–cellulose/Zn^{2+}/Ca^{2+}), dynamic hydrogen-bonded cross-linked networks, and metal ion coordination (Al^{3+}, Zn^{2+}) can optimize the continuity and deformation synchrony of conductive pathways, enabling sensitive resistance change responses. Meanwhile, the rapid breaking/reconstruction capability of dense dynamic bonds or efficient charge transfer across heterojunction interfaces helps reduce signal transmission delay and improve response speed. Additionally, the assembly method of the sensor (assembled vs. bare self-adhesive) also affects sensitivity, further highlighting the role of structural design in performance modulation.

In practical applications, the optimization of sensitivity and response time must align with specific scenario requirements. For instance, detecting subtle physiological signals (fine vibrations) demands high sensitivity to capture weak strains, while monitoring large-scale limb movements requires stable sensitivity across a wide strain range. Simultaneously, the response speed must match the strain rate of physiological activities or motions to ensure real-time and accurate signal acquisition [11,108,109]. These characteristics collectively determine the application potential of strain-sensing materials in fields such as flexible electronics, human–machine interaction, health monitoring, and intelligent robotics.

For CCH, Yue et al. [110] designed a CMOF@MoS_2 heterojunction by in situ growth of molybdenum disulfide (MoS_2) on a carbonized metal–organic framework (CMOF). They incorporated this heterojunction network into a hydrogel matrix containing sodium carboxymethyl cellulose and poly(vinyl alcohol), resulting in a CCH with high sensitivity (GF of 20.1 in the 0–150% strain range, 85.4 in the 150–250% range, and 97.1 in the 150–320% range) and rapid response characteristics (response time of 30 ms, recovery time of 23 ms) (Figure 6a). Zhu et al. [111] developed a CCH synthesized from carboxymethyl cellulose (CMC) interpenetrated within a polyacrylamide (PAAm) network. The resulting material demonstrated high sensitivity (GF = 3.15), a rapid real-time response (360 ms), and the ability to withstand 500 cycles at 300% strain (Figure 6b). Ni et al. [112] enhanced the CCH by incorporating quaternized cellulose nanofibers and MXene nanosheets into the matrix network. The high electrical conductivity of MXene, combined with the bridging effect of cellulose nanofibers, endowed the CCH with favorable sensitivity (GF: 0.45–2.24), a broad detection range (0–1465%), and excellent response–recovery capability (response and recovery time ≈140 ms) (Figure 6c). Inspired by human muscle, Lin et al. [113] utilized PVA and polypyrrole-decorated cellulose nanofibrils (PPy@CNF) as biocompatible polymers mimicking muscle fibers, with tannic acid (TA) serving as a hydrogen-bonded cross-linking medium. The resulting material achieved a maximum GF of 1.58, enabling

stable monitoring of multi-degree-of-freedom human joint movements and control of a multi-axis virtual robotic hand. Moreover, it exhibited stable electrical response signals even after 14 days of implantation in a mouse tendon. These works provide novel strategies for the development of integrated flexible smart microsystems that combine power supply, energy storage, and sensing functionalities.
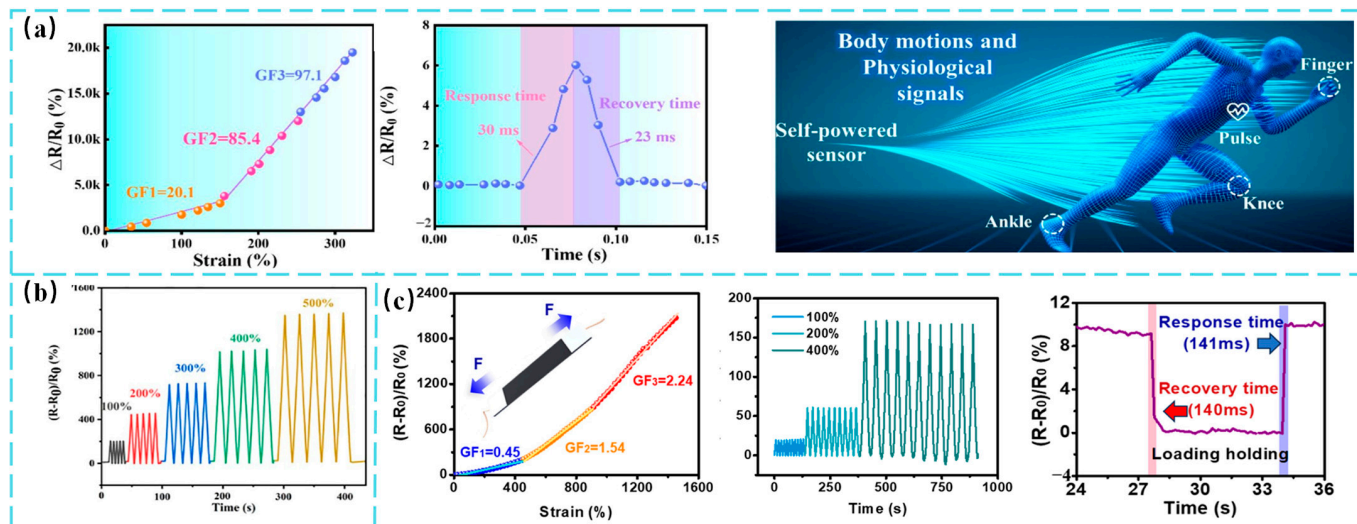

Figure 6. Strain-sensing performance and application demonstrations of CCHs. (**a**) Sensitivity of the CMOF@MoS$_2$ sensor as a function of strain; schematic illustration of response/recovery time and its assembly for intelligent healthcare monitoring (Reprinted with permission from [110]). (**b**) Resistance change in PAAm/CMC-CCH under various tensile strains at a stretching speed of 1.5 cm/s (Reprinted with permission from [111]). (**c**) Sensitivity of PAM-Q-CCH, relative resistance change under varying strain levels (100–400%), and response time during finger bending loading and unloading (Reprinted with permission from [112]).

For CCIG, Liu et al. [114] employed acrylic acid (AA), 2-methoxyethyl acrylate (MEA), sodium carboxymethyl cellulose (CMC), Al^{3+}, dimethyl sulfoxide (DMSO), and water as the main components in a dual-solvent organic CCIG. Under tensile strains ranging from 2.5% to 500%, the GF increased from 1.47 to 3.60, demonstrating sensitive and reliable strain sensing. The response and recovery times were approximately 400 ms and 600 ms, respectively, meeting the requirements for human motion detection (Figure 7a). Shu et al. [72] employed a simple one-pot method to dissolve 5 wt% PVA and cotton linter cellulose in a concentrated inorganic ZnCl$_2$/CaCl$_2$ solution, forming a dual-network CCIG. Owing to the effective "water-locking" effect of the polymer network, this CCIG exhibited the GF of 1.14 and a response time of approximately 200 ms at 75% relative resistance change, demonstrating rapid response and durable sensitivity to both tensile strain and compressive stress (Figure 7b). Wang et al. [115] developed a dual-network CCIG based on PVA/borax and cellulose/Zn^{2+}/Ca^{2+}, and evaluated two assembly methods: an assembled sensor and a bare self-adhesive sensor. The assembled strain sensor exhibited a rapid increase in GF, reaching a maximum value of 1.04 under strains up to 200%, and maintained a stable GF around 1 at higher applied strains up to 600%. It demonstrated reasonable response and recovery times of 268 ms and 346 ms, respectively. In contrast, the bare self-adhesive sensor showed GFs of 2.1 and 4 in the applied strain ranges of 0–100% and 100–600%, respectively (Figure 7c). These results indicate that the assembly process influences the material's sensitivity, while the dual-network cross-linked structure effectively ensures its promising potential for use in strain sensors and triboelectric nanogenerators under harsh conditions.
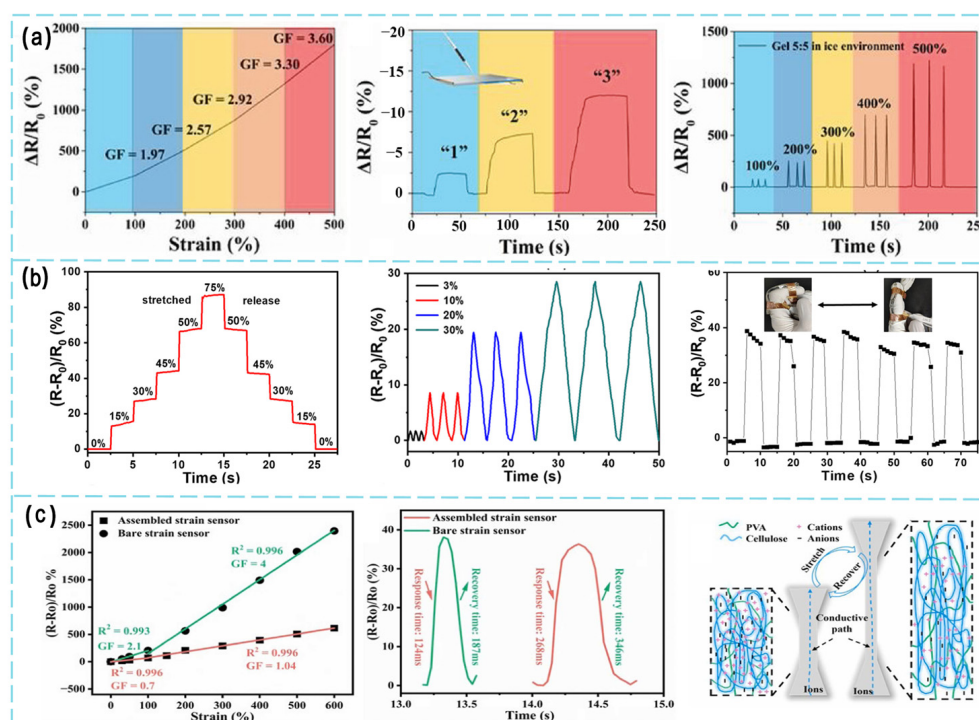
Figure 7. Strain-sensing performance and application demonstrations of CCIGs. (**a**) Sensitivity of gel-5 across different strain regions (2.5% to 500%); illustration of water writing on the gel surface and relative resistance changes in an icy environment within the 100% to 500% strain range (Reprinted with permission from [114]). (**b**) Relative resistance response of Gel-5 during cyclic strain from 0 to 100%, and relative resistance changes at different finger bending angles under varying strains (Reprinted with permission from [72]). (**c**) Relative resistance changes in assembled and bare self-adhesive strain sensors under applied strain; response and recovery times; schematic illustration of the sensing mechanism (Reprinted with permission from [115]).

For CICEs, Zhang et al. [74] developed CICEs with a dynamically cross-linked network formed through multiple hydrogen bonds. When as a strain sensor, it exhibited a three-stage response within the 0–300% strain range, with the GF of 1.59 in the 0–110% range, 2.66 in the 110–200% range, and 3.67 in the 200–300% range. The material demonstrated high sensitivity across a wide strain range. Under ultralow strain (1%) loading and unloading, it achieved a rapid response time of approximately 75 ms and a recovery time of about 70 ms (Figure 8a). Lu et al. [6] developed the CICEs based on a deep eutectic solvent (MDES) system comprising hydroxypropyl cellulose (HPC), ethylene glycol (EG), acrylic acid (AA), and $ZnCl_2$. This system achieved a response time as low as 42.8 ms, making it suitable for e-skin applications, given that human skin typically exhibits response times between 50 and 100 ms (Figure 8b). Luo et al. [116] synthesized a cellulose rosin-derived polyesterimide (PEI) through esterification and imidization reactions, and incorporated it into a polymerizable deep eutectic solvent (PDES) composed of choline chloride (ChCl) and 2-hydroxyethyl acrylate (HEA). The supramolecular hydrogen bonds formed between amine and hydroxyl groups in the system contributed to a gauge factor (GF) of 1.06 within the 0–300% strain range, along with a rapid response time (114 ms) and self-recovery capability (230 ms) at 100% strain (Figure 8c).

Table 3. A summary of strain-sensing metrics for representative CPIC-based sensors.

CPIC	Material	GF	Response Time(s)	Strain Range	Cyclic Stability	Reference
CCH	CMC + LiCl + AAM	3.15	360	1200%	500 cycles at a compressive strain of 300%	[111]
	QACNF + MXene	2.24	140	1465%	100 cycles at a compressive strain of 60%	[112]
	PVA + PPY + CNF + TA	1.92	400	414%	2000 cycles at a compressive strain of 30%	[113]
	cotton linter cellulose + ZnCl$_2$/CaCl$_2$ + PVA	1.14	200		50 cycles at a compressive strain of 50%	[72]
	MoS$_2$ + CMOF	20.1	23	320%	10,000 cycles at a compressive strain of 320%	[110]
	CNF + AAM + Mxenes + LiCl + Chitosan	4.17	130	800%		[117]
	CNC + PANI + PVA	2.56	7	1085%	Over 1000 cycles of wrist bending	[118]
	CMC + AM + FeCl$_3$	1.4	980	1086%		[119]
	CNF + PAM + PBA-IL	3.41	160	1810%	500 cycles at a compressive strain of 100%	[120]
	CMC + FeCl$_3$ + PAAm	1.99	260	690%	200 cycles at a tensile strain of 100%	[121]
	Methylcellulose + PAMC + TA@CNCs + LiCl	1.63	227	600.00%	300 cycles at a tensile strain of 100%	[122]
	BC + LiCl + DMAc + Mxene	1.51	130	120%	250 cycles at a tensile strain of 10%	[123]
	HECM + PAA + PPy	1.67	180.6	254%	1000 cycles at a tensile strain of 40%	[124]
	CNCs + AMM + BA + NaCl	7.4	140	750%	Continuous cyclic stretching-release for 700 s under a tensile strain of 300%	[125]
	CNC + PAM + rGO	3.4	125	400		[126]
CCIG	CMC + P(AA-MEA) + AlCl$_3$	1.47	400	500%	300 cycles at a tensile strain of 400%	[114]
	Cellulose + PVA + ZnCl$_2$ + CaCl$_2$	2.1	187	600%	10 cycles at a tensile strain of 100%	[115]
	Cellulose + [Bmim]Cl + P(AM-DMAA-MAA)	3.95	140	350%	100 cycles at a tensile strain of 40%	[127]
	CNF + PAZ + FeCl$_3$ + Gly	1.52	427	900%	500 cycles at a tensile strain of 30%	[128]
	CNF + PAZ + +LiCl + ZILs	1.98	142	1400%	100 cycles at a tensile strain of 100%	[129]
	BC + PAM + [EMIM]Cl	4.28	177.7	1000%	500 cycles at a tensile strain of 100%	[130]
	HPC + LA + AA + [C2VIm]Br	2.29		4222%	1000 cycles at a tensile strain of 50%	[31]
	HPC + PAA + [EMIM][DEP]	2.65	846	800%	300 cycles at a tensile strain of 40%	[131]
	PA + DES + [EMIM]BF$_4$	1.15		2500%	45 cycles at a tensile strain of 100%	[132]
CICEs	CNC + PAA + TA + ChCl	1.59	2400%	75	100 cycles at a tensile strain of 100%	[74]
	HPC + ZnCl$_2$ + EG + AA		197.70%	42.8	700 cycles at a tensile strain of 40%	[6]
	Cellulose + MCC-M-A + PDES	1.06	395%	114	500 cycles at a tensile strain of 15%	[116]
	EC-g-P(LMA-co-FMA) + ESOM + CNT	1.744	47.20%	277	200 cycles at a tensile strain of 25%	[133]
	SCNC + CNT + PDMS	10.77	100%		1000 cycles at a tensile strain of 50%	[134]
	C-CNC@PANI + ENR	1.45	300%	162.3	5 cycles at a tensile strain of 300%	[135]
	MCNF + CNT + SR	20.8	300%		510 cycles at a tensile strain of 100%	[136]
	CMC + S-PAM + LiCl + S-PDMS	3.8	70%		100 cycles at a tensile strain of 70%	[137]

Footer: CMC: Carboxymethyl Cellulose; LiCl: Lithium Chloride; AAM: Acrylamide; QACNF: Quaternized Cellulose Nanofibrils; MXene: Transition metal carbides/nitrides/carbonitrides (e.g., Ti$_3$C$_2$T$_X$); PVA: Polyvinyl Alcohol; PPY: Polypyrrole; CNF: Cellulose Nanofibrils; TA: Tannic Acid; ZnCl$_2$: Zinc Chloride; CaCl$_2$: Calcium Chloride; MoS$_2$: Molybdenum Disulfide; CMOF: Carbonized Metal–Organic Framework; Chitosan: Poly(β-(1→4)-2-amino-2-deoxy-D-glucose); CNC: Cellulose Nanocrystals; PANI: Polyaniline; AM: Acrylamide; FeCl$_3$: Iron(III) Chloride; PAM: Polyacrylamide; PBA-IL: Phenylboronic Acid-Functionalized Ionic Liquid; PAAm: Polyacrylamide; Methylcellulose: Cellulose methyl ether; PAMC: Poly(acrylamide-co-methylacrylate); TA@CNCs: Tannic Acid-coated Cellulose Nanocrystals; BC: Bacterial Cellulose; DMAc: N,N-Dimethylacetamide; HECM: Hydroxyethyl Cellulose Methacrylate; PAA: Poly(acrylic acid); AMM: Acrylamide-methacrylamide; BA: Butyl acrylate; NaCl: Sodium Chloride; rGO: Reduced Graphene Oxide; P(AA-MEA): Poly(acrylic acid-monoethanolamine); AlCl$_3$: Aluminum Chloride; [Bmim]Cl: 1-Butyl-3-methylimidazolium chloride; P(AM-DMAA-MAA): Poly(acrylamide-N,N-dimethylacrylamide-methacrylic acid); PAZ: Poly(acrylamide-Zn^{2+}); Gly: Glycerol; ZILs: Zwitterionic Ionic Liquids; [EMIM]Cl: 1-Ethyl-3-methylimidazolium chloride; HPC: Hydroxypropyl Cellulose; LA: Lipoic Acid; [C2VIm]Br: 1-Ethyl-2-vinylimidazolium bromide; [EMIM][DEP]: 1-Ethyl-3-methylimidazolium diethyl phosphate; PA: Polyacrylate; DES: Deep Eutectic Solvent; [EMIM]BF$_4$: 1-Ethyl-3-methylimidazolium tetrafluoroborate; ChCl: Choline Chloride; EG: Ethylene Glycol; MCC-M-A: Microcrystalline Cellulose-modified Rosin-based Polyimide; PDMS: Polydimethylsiloxane; EC-g-P(LMA-co-FMA): Ethyl Cellulose-g-poly(lauryl methacrylate-co-furfuryl methacrylate); ESOM: Maleimide-modified Epoxidized Soybean Oil; CNT: Carbon Nanotubes; SCNC: Silylated Cellulose Nanocrystals; C-CNC@PANI: Carboxylated Cellulose Nanocrystals@Polyaniline; ENR: Epoxidized Natural Rubber; MCNF: Vinyl Silane-modified Cellulose Nanofibrils; SR: Silicone Rubber; S-PAM: Silane-modified Polyacrylamide; S-PDMS: Silane-modified Polydimethylsiloxane.
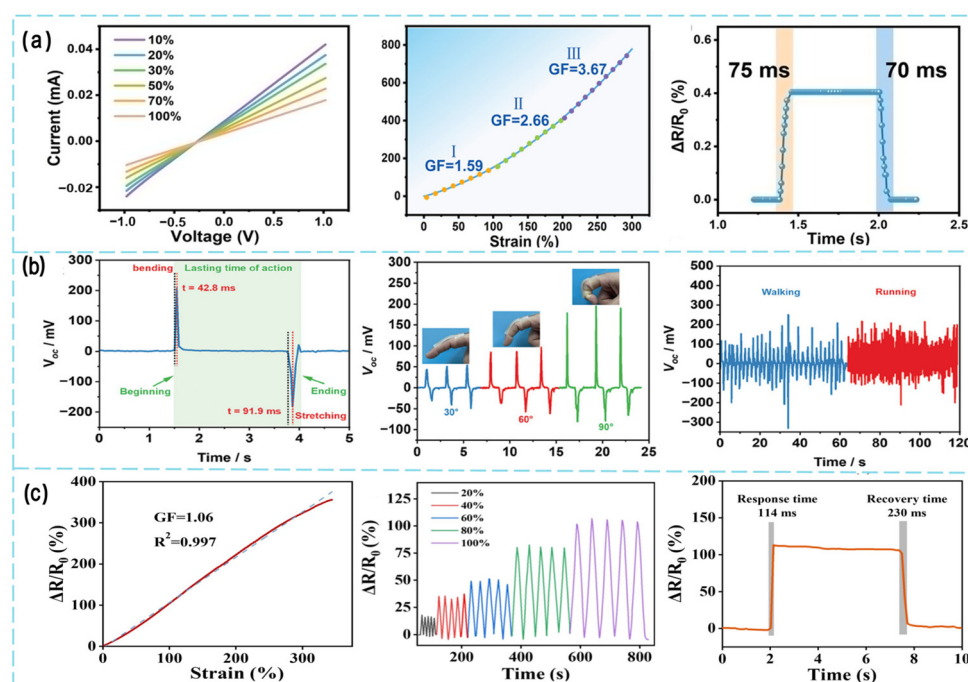
Figure 8. Strain-sensing performance and application demonstrations of CICEs. (**a**) Current–voltage curves of the CICE-based strain sensor under different tensile strains (from 10% to 100%) with voltage sweeping from −1.0 to 1.0 V; relative resistance change versus applied strain in the 0–300% range; and response and recovery time (Reprinted with permission from [74]). (**b**) Response time of the e-skin; relative voltage changes during finger bending, walking, and running motions (Reprinted with permission from [6]). (**c**) The GF of the PDES-CICE sensor under different strains; relative resistance change under continuous small strains (20–100%); and response and recovery time at 100% strain (Reprinted with permission from [116]).

7. Summary and Outlook

As the three major categories of CPICs, CCHs, CCIGs, and CICEs exhibit distinct characteristics and advantages. Among them, CCHs feature high water content and excellent biocompatibility, endowing it with significant potential for applications in flexible electronic devices and biomedical materials. CCIGs possess superior freeze resistance, low volatility, flame retardancy, high ionic conductivity, and thermal stability—properties that underpin its remarkable application prospects in flexible electronics, sensors, and environmental monitoring. CICEs have emerged as a research hotspot in solid-state batteries owing to their high energy density, compatibility with lithium metal anodes, and high conductivity. The development of these CPIC subtyped materials not only promotes the advancement and practical application of multifunctional materials in related fields but also offers novel solutions for sustainable and environmentally friendly material demands.

Despite their promising applications, CPICs still face several challenges. For instance, the freeze resistance of CCHs at low temperatures and its stability at elevated temperatures require further improvement. The high concentration of ionic liquids in CCIGs may compromise mechanical strength and pose potential leakage risks. The ionic conductivity of CICEs requires enhancement in both numerical magnitude and low-temperature stability—for example, in practical application scenarios where rapid ion migration is needed to achieve "real-time signal transmission" or "low-internal-resistance energy transfer," and where sharp declines in ionic conductivity below 0 °C must be mitigated to avoid functional failure. Their mechanical properties call for improvements in tensile strength, flexibility, and fatigue resistance: for instance, maintaining structural integrity and performance during repeated stretching or bending without brittle fracture, thus extending the material's

service life. Beyond subtype- associated issues, common bottlenecks across all CPIC include inadequate long-term stability, poor cycling durability, and suboptimal interfacial compatibility with electrodes—all of which are focal points of current research.

Future studies should focus on addressing these challenges through targeted material design and structural optimization to improve the overall performance of CPICs. Specific directions are proposed as follows: developing novel cross-linking strategies to enhance mechanical properties and fatigue resistance; exploring environmentally friendly additives and modification methods to improve environmental stability; investigating the interaction mechanisms between CPICs and electrodes to optimize interfacial compatibility; and designing new CPIC materials with high ionic conductivity, wide electrochemical windows, robust mechanical strength, and excellent interfacial stability. Furthermore, with the rapid development of the Internet of Things and wearable technology, optimizing the strain-sensing performance of CPICs will be particularly important for applications in flexible electronic skin, health monitoring, and human–machine interfaces.

In summary, research on CPICs not only holds theoretical significance and practical value for promoting the application of renewable resources in energy storage and conversion but also contributes profoundly to the development of an environmentally friendly and resource-efficient society. With continued advancements in materials science and energy conversion technologies, CPICs are expected to undergo significant improvements, expanding their application scope, and playing an increasingly vital role in addressing global energy challenges and driving sustainable human development.

Author Contributions: Conceptualization—R.L., P.Z. and Q.H.; formal analysis—R.L. and P.Z.; investigation, R.L. and Y.W.; writing—R.L., P.Z. and Q.H.; visualization—R.L., H.P. and P.Z.; review and editing—Y.W., P.Z. and Q.H. All authors have read and agreed to the published version of the manuscript.

Data Availability Statement: No new data were created or analyzed in this study. Data sharing is not applicable to this article.

Conflicts of Interest: The authors declare no conflicts of interest.

References

1. Jiang, L.; He, S.; Liu, A.; Zhang, J.; Liu, J.; He, S.; Shao, W. Preparation and characterization of self-healable and wearable hydrogels with ultrasensitive sensing performances. *Compos. Part B Eng.* **2022**, *239*, 109982. [CrossRef]
2. Wu, S.; Peng, S.; Yu, Y.; Wang, C.-H. Strategies for Designing Stretchable Strain Sensors and Conductors. *Adv. Mater. Technol.* **2020**, *5*, 1900908. [CrossRef]
3. Riess, I. Polymeric mixed ionic electronic conductors. *Solid State Ion.* **2000**, *136*, 1119–1130. [CrossRef]
4. Takada, A.; Kadokawa, J.-i. Preparation of cellulosic soft and composite materials using ionic liquid media and ion gels. *Cellulose* **2022**, *29*, 2745–2754. [CrossRef]
5. Li, X. Preparation of Lignocellulosic Hydrogel Electrolyte and Its Application in Supercapacitors. Master's Thesis, Northeast Forestry University, Harbin, China, 2023.
6. Lu, C.; Wang, X.; Shen, Y.; Xu, S.; Huang, C.; Wang, C.; Xie, H.; Wang, J.; Yong, Q.; Chu, F. Skin-like transparent, high resilience, low hysteresis, fatigue-resistant cellulose-based eutectogel for self-powered E-skin and human–machine interaction. *Adv. Funct. Mater.* **2024**, *34*, 2311502. [CrossRef]
7. Pei, X.; Zhang, H.; Zhou, Y.; Zhou, L.; Fu, J. Stretchable, self-healing and tissue-adhesive zwitterionic hydrogels as strain sensors for wireless monitoring of organ motions. *Mater. Horiz.* **2020**, *7*, 1872–1882. [CrossRef]
8. Dragan, E.S. Advances in interpenetrating polymer network hydrogels and their applications. *Pure Appl. Chem.* **2014**, *86*, 1707–1721. [CrossRef]

9. Ye, Y.; Yu, L.; Lizundia, E.; Zhu, Y.; Chen, C.; Jiang, F. Cellulose-based ionic conductor: An emerging material toward sustainable devices. *Chem. Rev.* **2023**, *123*, 9204–9264. [CrossRef]

10. Yang, Y.; Liu, Y.; Yin, R. Fiber/Yarn and Textile-Based Piezoresistive Pressure Sensors. *Adv. Fiber Mater.* **2025**, *7*, 34–71. [CrossRef]

11. Xi, J.; Yang, H.; Li, X.; Wei, R.; Zhang, T.; Dong, L.; Yang, Z.; Yuan, Z.; Sun, J.; Hua, Q. Recent advances in tactile sensory systems: Mechanisms, fabrication, and applications. *Nanomaterials* **2024**, *14*, 465. [CrossRef]

12. Taokaew, S.; Kriangkrai, W. Recent progress in processing cellulose using ionic liquids as solvents. *Polysaccharides* **2022**, *3*, 671–691. [CrossRef]

13. Ning, C.; Zhang, X.; Jiang, C.; Liu, W.; Sun, H.; Hou, Q. Study on Preparation and Properties of Nanocellulose-Polymerizable Deep Eutectic Solvents Ionic Conductive Elastomer. *China Pulp Pap.* **2023**, *42*, 43–49.

14. Porcarelli, L.; Gerbaldi, C.; Bella, F.; Nair, J.R. Super soft all-ethylene oxide polymer electrolyte for safe all-solid lithium batteries. *Sci. Rep.* **2016**, *6*, 19892. [CrossRef]

15. Chen, Z.; Du, J.; Wang, Y.; Li, Z.; Song, W.; Wei, R.; Chen, D.; Hua, Q.; Fu, X.; Huang, S. Fully Integrated Multifunctional Flexible Ultrasonic–Electric-Coupled Patches for Advancing Wound Care Paradigms. *Adv. Funct. Mater.* **2025**, *35*, 2425025. [CrossRef]

16. Cui, Z.; Hua, Q.; Shi, Y.; Wei, R.; Dong, Z.; Dai, X.; Huang, T.; Shen, G.; Wang, Z.L.; Hu, W. Skin-integrated haptic interface system based on a stretchable pressure sensor array for wireless tactile visualization applications. *Nano Energy* **2025**, *139*, 110911. [CrossRef]

17. Shen, J.; Fu, S. Research progress of cellulose-based hydrogels. *Chem. Ind. Eng. Prog.* **2022**, *41*, 3022–3037.

18. Fu, Q.; Liu, Y.; Mo, J.; Lu, Y.; Cai, C.; Zhao, Z.; Wang, S.; Nie, S. Improved capture and removal efficiency of gaseous acetaldehyde by a self-powered photocatalytic system with an external electric field. *ACS Nano* **2021**, *15*, 10577–10586. [CrossRef]

19. Chen, Z.; Liu, J.; Chen, Y.; Zheng, X.; Liu, H.; Li, H. Multiple-stimuli-responsive and cellulose conductive ionic hydrogel for smart wearable devices and thermal actuators. *ACS Appl. Mater. Interfaces* **2020**, *13*, 1353–1366. [CrossRef]

20. Chen, S.; Zhou, B.; Ma, M.; Wu, B.; Shi, Y.; Wang, X. Multiporous microstructure for enhancing the water absorption and swelling rate in poly (sodium acrylic acid) superabsorbent hydrogels based on a novel physical and chemical composite foaming system. *J. Appl. Polym. Sci.* **2016**, *133*. [CrossRef]

21. Yang, Y.; Xu, L.; Wang, J.; Meng, Q.; Zhong, S.; Gao, Y.; Cui, X. Recent advances in polysaccharide-based self-healing hydrogels for biomedical applications. *Carbohydr. Polym.* **2022**, *283*, 119161. [CrossRef] [PubMed]

22. Hu, Y.; Zhang, M.; Qin, C.; Qian, X.; Zhang, L.; Zhou, J.; Lu, A. Transparent, conductive cellulose hydrogel for flexible sensor and triboelectric nanogenerator at subzero temperature. *Carbohydr. Polym.* **2021**, *265*, 118078. [CrossRef]

23. Rathika, R.; Suthanthiraraj, S.A. Influence of 1-ethyl-3-methylimidazolium bis (trifluoromethyl sulfonyl) imide plasticization on zinc-ion conducting PEO/PVdF blend gel polymer electrolyte. *J. Mater. Sci. Mater. Electron.* **2018**, *29*, 19632–19643. [CrossRef]

24. Cho, K.G.; Kim, H.S.; Jang, S.S.; Kyung, H.; Kang, M.S.; Lee, K.H.; Yoo, W.C. Optimizing electrochemically active surfaces of carbonaceous electrodes for ionogel based supercapacitors. *Adv. Funct. Mater.* **2020**, *30*, 2002053. [CrossRef]

25. Ju, M.; Wu, B.; Sun, S.; Wu, P. Redox-active iron-citrate complex regulated robust coating-free hydrogel microfiber net with high environmental tolerance and sensitivity. *Adv. Funct. Mater.* **2020**, *30*, 1910387. [CrossRef]

26. Yan, C.-C.; Li, W.; Liu, Z.; Zheng, S.; Hu, Y.; Zhou, Y.; Guo, J.; Ou, X.; Li, Q.; Yu, J.; et al. Ionogels: Preparation, Properties and Applications. *Adv. Funct. Mater.* **2024**, *34*, 2314408. [CrossRef]

27. Lei, Z.; Chen, B.; Koo, Y.-M.; MacFarlane, D.R. Introduction: Ionic liquids. *Chem. Rev.* **2017**, *117*, 6633–6635. [CrossRef] [PubMed]

28. Andrzejewska, E.; Marcinkowska, A.; Zgrzeba, A. Ionogels–materials containing immobilized ionic liquids. *Polimery* **2017**, *62*, 344–352. [CrossRef]

29. Chen, Q.; Liu, X.; Yang, J.; Tao, T.; Chen, L.; Ni, Y.; Li, J. Preparation and properties of cellulose ionic gel. *Acta Mater. Compos. Sin.* **2021**, *38*, 4247–4254.

30. Kong, L.; Lu, R.; Wang, Y.; Ran, Y.; Jv, J.; Sui, W.; Peng, Y. Transparent bamboo as a replacement for glass: Effects of lignin decolorisation methods on weatherability. *Int. J. Biol. Macromol.* **2024**, *277*, 134470. [CrossRef]

31. Liu, J.; Jiang, B.; Ji, J.; Cheng, F.; Cai, C.; Fu, Y. Unmatched resilience and fatigue resistance in a novel cellulose-derived ionic gel with hierarchical superstructured synergy for advanced human-computer interaction. *Chem. Eng. J.* **2024**, *497*, 154672. [CrossRef]

32. Li, Z.; Fu, J.; Zhou, X.; Gui, S.; Wei, L.; Yang, H.; Li, H.; Guo, X. Ionic conduction in polymer-based solid electrolytes. *Adv. Sci.* **2023**, *10*, 2201718. [CrossRef]

33. Zhou, D.; Shanmukaraj, D.; Tkacheva, A.; Armand, M.; Wang, G. Polymer electrolytes for lithium-based batteries: Advances and prospects. *Chem* **2019**, *5*, 2326–2352. [CrossRef]

34. Li, S.; Zhang, S.Q.; Shen, L.; Liu, Q.; Ma, J.B.; Lv, W.; He, Y.B.; Yang, Q.H. Progress and perspective of ceramic/polymer composite solid electrolytes for lithium batteries. *Adv. Sci.* **2020**, *7*, 1903088. [CrossRef]

35. Wang, D.; Xie, H.; Liu, Q.; Mu, K.; Song, Z.; Xu, W.; Tian, L.; Zhu, C.; Xu, J. Low-Cost, High-Strength Cellulose-based Quasi-Solid Polymer Electrolyte for Solid-State Lithium-Metal Batteries. *Angew. Chem. Int. Ed.* **2023**, *62*, e202302767. [CrossRef]

36. Fu, Y.; Yang, L.; Zhang, M.; Lin, Z.; Shen, Z. Recent advances in cellulose-based polymer electrolytes. *Cellulose* **2022**, *29*, 8997–9034. [CrossRef]

37. Cheng, Y.; Cai, Z.; Xu, J.; Sun, Z.; Wu, X.; Han, J.; Wang, Y.-H.; Wang, M.-S. Zwitterionic Cellulose-Based Polymer Electrolyte Enabled by Aqueous Solution Casting for High-Performance Solid-State Batteries. *Angew. Chem. Int. Ed.* **2024**, *63*, e202400477. [CrossRef]

38. Gao, C. Construction of Composite Polymer Electrolytes Based onCellulose Derivatives and Performance in Lithium Batteries. Ph.D. Thesis, Shaanxi University of Science and Technology, Xi'an, China, 2023.

39. Jinisha, B.; Anilkumar, K.; Manoj, M.; Pradeep, V.; Jayalekshmi, S. Development of a novel type of solid polymer electrolyte for solid state lithium battery applications based on lithium enriched poly (ethylene oxide)(PEO)/poly (vinyl pyrrolidone)(PVP) blend polymer. *Electrochim. Acta* **2017**, *235*, 210–222.

40. Mindemark, J.; Törmä, E.; Sun, B.; Brandell, D. Copolymers of trimethylene carbonate and ε-caprolactone as electrolytes for lithium-ion batteries. *Polymer* **2015**, *63*, 91–98. [CrossRef]

41. Liu, F.; Bin, F.; Xue, J.; Wang, L.; Yang, Y.; Huo, H.; Zhou, J.; Li, L. Polymer electrolyte membrane with high ionic conductivity and enhanced interfacial stability for lithium metal battery. *ACS Appl. Mater. Interfaces* **2020**, *12*, 22710–22720. [CrossRef] [PubMed]

42. Chen, J.; Wang, J.; Ji, K.; Jiang, B.; Cui, X.; Sha, W.; Wang, B.; Dai, X.; Hua, Q.; Wan, L. Flexible, stretchable, and transparent InGaN/GaN multiple quantum wells/polyacrylamide hydrogel-based light emitting diodes. *Nano Res.* **2022**, *15*, 5492–5499. [CrossRef]

43. Dey, K.; Agnelli, S.; Borsani, E.; Sartore, L. Degradation-dependent stress relaxing semi-interpenetrating networks of hydroxyethyl cellulose in gelatin-PEG hydrogel with good mechanical stability and reversibility. *Gels* **2021**, *7*, 277. [CrossRef]

44. Zhao, D.; Huang, J.; Zhong, Y.; Li, K.; Zhang, L.; Cai, J. High-strength and high-toughness double-cross-linked cellulose hydrogels: A new strategy using sequential chemical and physical cross-linking. *Adv. Funct. Mater.* **2016**, *26*, 6279–6287. [CrossRef]

45. Rana, H.H.; Park, J.H.; Gund, G.S.; Park, H.S. Highly conducting, extremely durable, phosphorylated cellulose-based ionogels for renewable flexible supercapacitors. *Energy Storage Mater.* **2020**, *25*, 70–75. [CrossRef]

46. Kale, S.B.; Nirmale, T.C.; Khupse, N.D.; Kale, B.B.; Kulkarni, M.V.; Pavitran, S.; Gosavi, S.W. Cellulose-derived flame-retardant solid polymer electrolyte for lithium-ion batteries. *ACS Sustain. Chem. Eng.* **2021**, *9*, 1559–1567. [CrossRef]

47. Villar-Chavero, M.M.; Dominguez, J.C.; Alonso, M.V.; Oliet, M.; Rodriguez, F. Chitosan-reinforced cellulosic bionogels: Viscoelastic and antibacterial properties. *Carbohydr. Polym.* **2020**, *229*, 115569. [CrossRef]

48. Kunchornsup, W.; Sirivat, A. Electromechanical properties study of 1-butyl-3-methylimidazolium chloride/cellulosic gel blended with polydiphenylamine. *Sens. Actuators A Phys.* **2014**, *220*, 249–261. [CrossRef]

49. Lee, H.; Erwin, A.; Buxton, M.L.; Kim, M.; Stryutsky, A.V.; Shevchenko, V.V.; Sokolov, A.P.; Tsukruk, V.V. Shape persistent, highly conductive ionogels from ionic liquids reinforced with cellulose nanocrystal network. *Adv. Funct. Mater.* **2021**, *31*, 2103083. [CrossRef]

50. Song, H.; Luo, Z.; Zhao, H.; Luo, S.; Wu, X.; Gao, J.; Wang, Z. High tensile strength and high ionic conductivity bionanocomposite ionogels prepared by gelation of cellulose/ionic liquid solutions with nano-silica. *RSC Adv.* **2013**, *3*, 11665–11675. [CrossRef]

51. Chen, S.; Wang, H.-Z.; Zhao, R.-Q.; Rao, W.; Liu, J. Liquid metal composites. *Matter* **2020**, *2*, 1446–1480. [CrossRef]

52. Liu, X.; Taiwo, O.O.; Yin, C.; Ouyang, M.; Chowdhury, R.; Wang, B.; Wang, H.; Wu, B.; Brandon, N.P.; Wang, Q. Aligned ionogel electrolytes for high-temperature supercapacitors. *Adv. Sci.* **2019**, *6*, 1801337. [CrossRef]

53. Kunchornsup, W.; Sirivat, A. Effects of crosslinking ratio and aging time on properties of physical and chemical cellulose gels via 1-butyl-3-methylimidazolium chloride solvent. *J. Sol-Gel Sci. Technol.* **2010**, *56*, 19–26. [CrossRef]

54. Zhang, L.M.; He, Y.; Cheng, S.; Sheng, H.; Dai, K.; Zheng, W.J.; Wang, M.X.; Chen, Z.S.; Chen, Y.M.; Suo, Z. Self-healing, adhesive, and highly stretchable ionogel as a strain sensor for extremely large deformation. *Small* **2019**, *15*, 1804651. [CrossRef]

55. Huang, F.; Wei, W.; Fan, Q.; Li, L.; Zhao, M.; Zhou, Z. Super-stretchable and adhesive cellulose Nanofiber-reinforced conductive nanocomposite hydrogel for wearable Motion-monitoring sensor. *J. Colloid Interface Sci.* **2022**, *615*, 215–226. [CrossRef]

56. Shu, L.; Wang, Z.; Zhang, X.-F.; Yao, J. Highly conductive and anti-freezing cellulose hydrogel for flexible sensors. *Int. J. Biol. Macromol.* **2023**, *230*, 123425. [CrossRef]

57. Cheng, H.; Fan, Z.; Wang, Z.; Guo, Z.; Jiang, J.; Xie, Y. Highly stretchable, fast self-healing nanocellulose hydrogel combining borate ester bonds and acylhydrazone bonds. *Int. J. Biol. Macromol.* **2023**, *245*, 125471. [CrossRef]

58. Zhang, Y.; Sun, X.; Ye, Y.; Oguzlu, H.; Zhu, Y.; Zhu, J.; Le, K.; Yang, P.; Jiang, F. All-cellulose hydrogel with ultrahigh stretchability exceeding 40000%. *Mater. Today* **2024**, *74*, 67–76. [CrossRef]

59. Wang, M.; Hu, J.; Dickey, M.D. Tough ionogels: Synthesis, toughening mechanisms, and mechanical properties—A perspective. *JACS Au* **2022**, *2*, 2645–2657. [CrossRef]

60. Long, Q.; Jiang, G.; Zhou, J.; Zhao, D.; Yu, H. A cellulose ionogel with rubber-like stretchability for low-grade heat harvesting. *Research* **2024**, *7*, 0533. [CrossRef] [PubMed]

61. Jiang, H.; Bai, R.; Zhao, Y.; Shi, S.; Jiang, G.; Zhao, D. Mechanically robust, highly conductive, wide-voltage cellulose ionogels enabled by molecular network reconstruction. *Adv. Funct. Mater.* **2025**, *35*, 2503512. [CrossRef]

62. Guo, S.; Zhao, K.; Feng, Z.; Hou, Y.; Li, H.; Zhao, J.; Tian, Y.; Song, H. High performance liquid crystalline bionanocomposite ionogels prepared by in situ crosslinking of cellulose/halloysite nanotubes/ionic liquid dispersions and its application in supercapacitors. *Appl. Surf. Sci.* **2018**, *455*, 599–607. [CrossRef]

63. Chen, W.; Bu, Y.; Li, D.; Liu, C.; Chen, G.; Wan, X.; Li, N. High-strength, tough, and self-healing hydrogel based on carboxymethyl cellulose. *Cellulose* **2020**, *27*, 853–865. [CrossRef]

64. Colò, F.; Bella, F.; Nair, J.R.; Destro, M.; Gerbaldi, C. Cellulose-based novel hybrid polymer electrolytes for green and efficient Na-ion batteries. *Electrochim. Acta* **2015**, *174*, 185–190. [CrossRef]

65. Zhou, W.; Wang, S.; Li, Y.; Xin, S.; Manthiram, A.; Goodenough, J.B. Plating a dendrite-free lithium anode with a polymer/ceramic/polymer sandwich electrolyte. *J. Am. Chem. Soc.* **2016**, *138*, 9385–9388. [CrossRef]

66. Zhao, X.; Wang, W.; Huang, C.; Luo, L.; Deng, Z.; Guo, W.; Xu, J.; Meng, Z. A novel cellulose membrane from cattail fibers as separator for Li-ion batteries. *Cellulose* **2021**, *28*, 9309–9321. [CrossRef]

67. Deng, L.; Wang, Y.; Cai, C.; Wei, Z.; Fu, Y. 3D-cellulose acetate-derived hierarchical network with controllable nanopores for superior Li+ transference number, mechanical strength and dendrites hindrance. *Carbohydr. Polym.* **2021**, *274*, 118620. [CrossRef]

68. Wang, S.; Zhang, L.; Ma, R.; Yu, J.; Zhang, X.; Shi, C.; Ma, L.; Li, T.; Huang, Y.; Hu, Y. A novel one-pot strategy to construct 3D-printable cellulose nanofiber/poly (deep eutectic solvent) conductive elastomers. *Chem. Eng. J.* **2023**, *454*, 140022. [CrossRef]

69. Wang, X.; Wei, R.; Chen, Z.; Pang, H.; Li, H.; Yang, Y.; Hua, Q.; Shen, G. Bioinspired Intelligent Soft Robotics: From Multidisciplinary Integration to Next-Generation Intelligence. *Adv. Sci.* **2025**, *12*, e06296. [CrossRef] [PubMed]

70. Peng, D.; Li, H.; Sun, J.; Deng, Y.; Jiao, F.; Han, Y.; Zhang, K.; Meng, J.; Li, X.; Wang, L. All-Optical Synapses Based on a Mechanoluminescent Material. *Adv. Mater.* **2025**, *37*, 2503376. [CrossRef]

71. Wei, R.; Li, H.; Chen, Z.; Hua, Q.; Shen, G.; Jiang, K. Revolutionizing wearable technology: Advanced fabrication techniques for body-conformable electronics. *npj Flex. Electron.* **2024**, *8*, 83. [CrossRef]

72. Shu, L.; Zhang, X.-F.; Wu, Y.; Wang, Z.; Yao, J. Facile fabrication of strong and conductive cellulose hydrogels with wide temperature tolerance for flexible sensors. *Int. J. Biol. Macromol.* **2023**, *240*, 124438. [CrossRef]

73. Li, X.; Song, X.; Qie, X.; Feng, H.; Min, Z.; Zhang, J.; Ren, S.; Ren, J. Tough and highly stretchable multifunctional ionogels based on phase-separated structure and nanocellulose macromolecular covalent cross-linker. *Cell Rep. Phys. Sci.* **2024**, *5*, 102073. [CrossRef]

74. Zhang, X.; Fu, Q.; Wang, Y.; Zhao, H.; Hao, S.; Ma, C.; Xu, F.; Yang, J. Tough liquid-free ionic conductive elastomers with robust adhesion and self-healing properties for ionotronic devices. *Adv. Funct. Mater.* **2024**, *34*, 2307400. [CrossRef]

75. Yin, L.; Zhang, P.; Yang, J.; Meng, J.; Wu, M.; Pu, X. A Dual-Bond Crosslinking Strategy Enabling Resilient and Recyclable Electrolyte Elastomers for Solid-State Lithium Metal Batteries. *Angew. Chem. Int. Ed.* **2024**, *63*, e202404769. [CrossRef]

76. Hu, L.; Chee, P.L.; Sugiarto, S.; Yu, Y.; Shi, C.; Yan, R.; Yao, Z.; Shi, X.; Zhi, J.; Kai, D.; et al. Hydrogel-Based Flexible Electronics. *Adv. Mater.* **2023**, *35*, 2205326. [CrossRef]

77. Zhang, X.F.; Ma, X.; Hou, T.; Guo, K.; Yin, J.; Wang, Z.; Shu, L.; He, M.; Yao, J. Inorganic salts induce thermally reversible and anti-freezing cellulose hydrogels. *Angew. Chem. Int. Ed.* **2019**, *58*, 7366–7370. [CrossRef]

78. Li, L.; Lu, F.; Wang, C.; Zhang, F.; Liang, W.; Kuga, S.; Dong, Z.; Zhao, Y.; Huang, Y.; Wu, M. Flexible double-cross-linked cellulose-based hydrogel and aerogel membrane for supercapacitor separator. *J. Mater. Chem. A* **2018**, *6*, 24468–24478. [CrossRef]

79. Yan, X.; Lin, X.; Liu, H.; Lu, J.; Wang, H.; Huang, X.; Liu, H.; Xu, X. Tough and temperature-tolerance cellulose/polyacrylic acid/bentonite hydrogel with high ionic conductivity enables self-powered triboelectric wearable electronic devices. *Carbohydr. Polym.* **2024**, *344*, 122552. [CrossRef] [PubMed]

80. Wang, S.; Yu, L.; Wang, S.; Zhang, L.; Chen, L.; Xu, X.; Song, Z.; Liu, H.; Chen, C. Strong, tough, ionic conductive, and freezing-tolerant all-natural hydrogel enabled by cellulose-bentonite coordination interactions. *Nat. Commun.* **2022**, *13*, 3408. [CrossRef] [PubMed]

81. Wang, Y.; Zhang, L.; Lu, A. Transparent, antifreezing, ionic conductive cellulose hydrogel with stable sensitivity at subzero temperature. *ACS Appl. Mater. Interfaces* **2019**, *11*, 41710–41716. [CrossRef]

82. Chen, D.; Zhao, X.; Wei, X.; Zhang, J.; Wang, D.; Lu, H.; Jia, P. Ultrastretchable, tough, antifreezing, and conductive cellulose hydrogel for wearable strain sensor. *ACS Appl. Mater. Interfaces* **2020**, *12*, 53247–53256. [CrossRef]

83. Cao, K.; Zhu, Y.; Zheng, Z.; Cheng, W.; Zi, Y.; Zeng, S.; Zhao, D.; Yu, H. Bio-inspired multiscale design for strong and tough biological ionogels. *Adv. Sci.* **2023**, *10*, 2207233. [CrossRef]

84. Zhao, D.; Zhu, Y.; Cheng, W.; Xu, G.; Wang, Q.; Liu, S.; Li, J.; Chen, C.; Yu, H.; Hu, L. A dynamic gel with reversible and tunable topological networks and performances. *Matter* **2020**, *2*, 390–403. [CrossRef]

85. Yim, C.-H.; Tam, J.; Soboleski, H.; Abu-Lebdeh, Y. On the correlation between free volume, phase diagram and ionic conductivity of aqueous and non-aqueous lithium battery electrolyte solutions over a wide concentration range. *J. Electrochem. Soc.* **2017**, *164*, A1002. [CrossRef]

86. Han, J.; Mariani, A.; Passerini, S.; Varzi, A. A perspective on the role of anions in highly concentrated aqueous electrolytes. *Energy Environ. Sci.* **2023**, *16*, 1480–1501. [CrossRef]

87. Zhang, J.; Yue, L.; Hu, P.; Liu, Z.; Qin, B.; Zhang, B.; Wang, Q.; Ding, G.; Zhang, C.; Zhou, X. Taichi-inspired rigid-flexible coupling cellulose-supported solid polymer electrolyte for high-performance lithium batteries. *Sci. Rep.* **2014**, *4*, 6272. [CrossRef] [PubMed]

88. Zhou, M.; Liu, R.; Jia, D.; Cui, Y.; Liu, Q.; Liu, S.; Wu, D. Ultrathin yet robust single lithium-ion conducting quasi-solid-state polymer-brush electrolytes enable ultralong-life and dendrite-free lithium-metal batteries. *Adv. Mater.* **2021**, *33*, 2100943. [CrossRef] [PubMed]

89. Zhang, Z.; Jin, J.; Bautista, F.; Lyons, L.; Shariatzadeh, N.; Sherlock, D.; Amine, K.; West, R. Ion conductive characteristics of cross-linked network polysiloxane-based solid polymer electrolytes. *Solid State Ion.* **2004**, *170*, 233–238. [CrossRef]

90. Wang, Y.; Zhong, W.H.; Schiff, T.; Eyler, A.; Li, B. A Particle-Controlled, High-Performance, Gum-Like Electrolyte for Safe and Flexible Energy Storage Devices. *Adv. Energy Mater.* **2015**, *5*, 1400463. [CrossRef]

91. Zhang, Y.; Wang, X.; Feng, W.; Zhen, Y.; Zhao, P.; Cai, Z.; Li, L. Effects of the shapes of $BaTiO_3$ nanofillers on PEO-based electrolytes for all-solid-state lithium-ion batteries. *Ionics* **2019**, *25*, 1471–1480. [CrossRef]

92. Zhang, Y.; Zhao, Y.; Gosselink, D.; Chen, P. Synthesis of poly (ethylene-oxide)/nanoclay solid polymer electrolyte for all solid-state lithium/sulfur battery. *Ionics* **2015**, *21*, 381–385. [CrossRef]

93. Kang, Y.; Lee, J.; Lee, J.-I.; Lee, C. Ionic conductivity and electrochemical properties of cross-linked solid polymer electrolyte using star-shaped siloxane acrylate. *J. Power Sources* **2007**, *165*, 92–96. [CrossRef]

94. Tian, Y.; Zhang, L.; Li, X.; Yan, M.; Wang, Y.; Ma, J.; Wang, Z. Compressible, anti-freezing, and ionic conductive cellulose/polyacrylic acid composite hydrogel prepared via $AlCl_3/ZnCl_2$ aqueous system as solvent and catalyst. *Int. J. Biol. Macromol.* **2023**, *253*, 126550. [CrossRef]

95. Li, N.; Qiu, Y.; Ma, J.; Qiu, L.; Sun, W.; Li, J.; Han, Z.; Chen, W.; Ji, X. Mechanically robust and multifunctional ionogels based on cellulose and polymerizable 1-butyl-3-methylimidazolium chloride/acrylamide deep eutectic solvent. *ACS Appl. Polym. Mater.* **2023**, *5*, 9974–9986. [CrossRef]

96. Wu, D.; Wang, M.; Yu, W.; Wang, G.-G.; Zhang, J. A robust, biodegradable and recyclable all-cellulose ionogel from low-value wood. *Chem. Eng. J.* **2024**, *486*, 150121. [CrossRef]

97. Li, J.; Hu, Z.; Zhang, S.; Zhang, H.; Guo, S.; Zhong, G.; Qiao, Y.; Peng, Z.; Li, Y.; Chen, S. Molecular engineering of renewable cellulose biopolymers for solid-state battery electrolytes. *Nat. Sustain.* **2024**, *7*, 1481–1491. [CrossRef]

98. Xu, Y.; Cui, J.; Guo, B.; Li, Z.; Wang, W.; Li, W. Cellulose-based eutectogel electrolyte with high ionic conductivity for solid-state lithium-ion batteries. *Chem. Eng. J.* **2024**, *491*, 151783. [CrossRef]

99. Wang, R.; Dong, W.; Song, Z.; Tan, J.; Liu, Q.; Mu, K.; Xu, W.; Huang, H.; Zhang, Z.; Yin, G. Ion-Conducting Molecular-Grafted Sustainable Cellulose Quasi-Solid Composite Electrolyte for High Stability Solid-State Lithium-Metal Batteries. *Adv. Funct. Mater.* **2024**, *34*, 2402461. [CrossRef]

100. Wang, Y.; Zhang, L.; Lu, A. Highly stretchable, transparent cellulose/PVA composite hydrogel for multiple sensing and triboelectric nanogenerators. *J. Mater. Chem. A* **2020**, *8*, 13935–13941. [CrossRef]

101. Wu, R.; Wang, Y.; Liu, Y.; Yuan, B. Functionalizing chitosan-based film with highly sensitive fire response and commendable flame retardancy for intelligent fire-alarm system. *Compos. Part A Appl. Sci. Manuf.* **2024**, *178*, 107999. [CrossRef]

102. Zhao, D.; Pang, B.; Zhu, Y.; Cheng, W.; Cao, K.; Ye, D.; Si, C.; Xu, G.; Chen, C.; Yu, H. A stiffness-switchable, biomimetic smart material enabled by supramolecular reconfiguration. *Adv. Mater.* **2022**, *34*, 2107857. [CrossRef]

103. Wang, Z.; Liu, J.; Zhang, J.; Hao, S.; Duan, X.; Song, H.; Zhang, J. Novel chemically cross-linked chitosan-cellulose based ionogel with self-healability, high ionic conductivity, and high thermo-mechanical stability. *Cellulose* **2020**, *27*, 5121–5133. [CrossRef]

104. Li, X.; Jiang, H.; Zhang, Y.; Long, Q.; Jiang, G.; Zeng, S.; Zhou, J.; Zhao, D. Stimulation-Reinforced Cellulose–Protein Ionogels with Superior Mechanical Strength and Temperature Resistance. *Adv. Funct. Mater.* **2024**, *34*, 2408160. [CrossRef]

105. Kotobuki, M.; Suzuki, Y.; Munakata, H.; Kanamura, K.; Sato, Y.; Yamamoto, K.; Yoshida, T. Electrochemical property of honeycomb type all-solid-state Li battery at high temperature. *Electrochemistry* **2011**, *79*, 464–466. [CrossRef]

106. Samad, Y.A.; Asghar, A.; Lalia, B.S.; Hashaikeh, R. Networked cellulose entrapped and reinforced PEO-based solid polymer electrolyte for moderate temperature applications. *J. Appl. Polym. Sci.* **2013**, *129*, 2998–3006. [CrossRef]

107. Wang, S.; Chen, Y.; Zhou, X.; Hu, B.; Wang, Y.; Li, Y.; Jing, X. Research Progress in Conducting Polymer Hydrogels and Their StrainSensing Properties. *Mater. Rep.* **2024**, *38*, 22120184-11.

108. Wang, B.; Shi, Y.; Li, H.; Hua, Q.; Ji, K.; Dong, Z.; Cui, Z.; Huang, T.; Chen, Z.; Wei, R. Body-Integrated Ultrasensitive All-Textile Pressure Sensors for Skin-Inspired Artificial Sensory Systems. *Small Sci.* **2024**, *4*, 2400026. [CrossRef]

109. Wang, S.; Yang, T.; Zhang, D.; Hua, Q.; Zhao, Y. Unveiling gating behavior in piezoionic effect: Toward neuromimetic tactile sensing. *Adv. Mater.* **2024**, *36*, 2405391. [CrossRef] [PubMed]

110. Yue, J.; Li, C.; Tao, Y.; Hu, J.; Lu, J.; Du, J.; Wang, H. Synergistic defect and heterojunction engineering of carbonized MOF@ MoS_2 for self-powered sensing micro-system with photothermal therapy. *Chem. Eng. J.* **2024**, *495*, 153367. [CrossRef]

111. Zhu, T.; Cheng, Y.; Cao, C.; Mao, J.; Li, L.; Huang, J.; Gao, S.; Dong, X.; Chen, Z.; Lai, Y. A semi-interpenetrating network ionic hydrogel for strain sensing with high sensitivity, large strain range, and stable cycle performance. *Chem. Eng. J.* **2020**, *385*, 123912. [CrossRef]

112. Ni, Q.-Y.; He, X.-F.; Zhou, J.-L.; Yang, Y.-Q.; Zeng, Z.-F.; Mao, P.-F.; Luo, Y.-H.; Xu, J.-M.; Jiang, B.; Wu, Q. Mechanical tough and stretchable quaternized cellulose nanofibrils/MXene conductive hydrogel for flexible strain sensor with multi-scale monitoring. *J. Mater. Sci. Technol.* **2024**, *191*, 181–191. [CrossRef]

113. Lin, F.; Yang, W.; Lu, B.; Xu, Y.; Chen, J.; Zheng, X.; Liu, S.; Lin, C.; Zeng, H.; Huang, B. Muscle-Inspired Robust Anisotropic Cellulose Conductive Hydrogel for Multidirectional Strain Sensors and Implantable Bioelectronics. *Adv. Funct. Mater.* **2025**, *35*, 2416419. [CrossRef]

114. Liu, J.; Chen, Z.; Chen, Y.; Rehman, H.U.; Guo, Y.; Li, H.; Liu, H. Ionic conductive organohydrogels with dynamic pattern behavior and multi-environmental stability. *Adv. Funct. Mater.* **2021**, *31*, 2101464. [CrossRef]

115. Wang, Y.; Zhang, Y.; Ren, P.; Yu, S.; Cui, P.; Nielsen, C.B.; Abrahams, I.; Briscoe, J.; Lu, Y. Versatile and recyclable double-network PVA/cellulose hydrogels for strain sensors and triboelectric nanogenerators under harsh conditions. *Nano Energy* **2024**, *125*, 109599. [CrossRef]

116. Luo, T.; Guo, X.; Qi, J.; Yu, J.; Lu, C.; Wang, C.; Chu, F.; Wang, J. Fabrication of liquid-free ionic conductive elastomer (ICE) from cellulose-rosin derived poly (esterimide) towards temperature-tolerant and solvent-resistant UV shadowless adhesive and sensor. *Int. J. Biol. Macromol.* **2024**, *278*, 134921. [CrossRef]

117. Geng, L.; Liu, W.; Fan, B.; Wu, J.; Shi, S.; Huang, A.; Hu, J.; Peng, X. Anisotropic double-network hydrogels integrated superior performance of strength, toughness and conductivity for flexible multi-functional sensors. *Chem. Eng. J.* **2023**, *462*, 142226. [CrossRef]

118. Song, M.; Yu, H.; Zhu, J.; Ouyang, Z.; Abdalkarim, S.Y.H.; Tam, K.C.; Li, Y. Constructing stimuli-free self-healing, robust and ultrasensitive biocompatible hydrogel sensors with conductive cellulose nanocrystals. *Chem. Eng. J.* **2020**, *398*, 125547. [CrossRef]

119. Cheng, Y.; Ren, X.; Gao, G.; Duan, L. High strength, anti-freezing and strain sensing carboxymethyl cellulose-based organohydrogel. *Carbohydr. Polym.* **2019**, *223*, 115051. [CrossRef]

120. Yao, X.; Zhang, S.; Qian, L.; Wei, N.; Nica, V.; Coseri, S.; Han, F. Super stretchable, self-healing, adhesive ionic conductive hydrogels based on tailor-made ionic liquid for high-performance strain sensors. *Adv. Funct. Mater.* **2022**, *32*, 2204565. [CrossRef]

121. Zhang, H.; Wu, X.; Qin, Z.; Sun, X.; Zhang, H.; Yu, Q.; Yao, M.; He, S.; Dong, X.; Yao, F. Dual physically cross-linked carboxymethyl cellulose-based hydrogel with high stretchability and toughness as sensitive strain sensors. *Cellulose* **2020**, *27*, 9975–9989. [CrossRef]

122. Gao, J.; Li, X.; Xu, L.; Yan, M.; Bi, H.; Wang, Q. Transparent multifunctional cellulose-based conductive hydrogel for wearable strain sensors and arrays. *Carbohydr. Polym.* **2024**, *329*, 121784. [CrossRef]

123. Gai, Y.; Yang, L.; Shen, W.; Tan, F.; Yu, Q.; Zhang, L.; Sun, D. A flexible piezoresistive strain sensor based on MXene/bacterial cellulose hydrogel with high mechanical strength for real-time monitoring of human motions. *J. Mater. Chem. C* **2024**, *12*, 1763–1772. [CrossRef]

124. Sun, W.; Liu, X.; Hua, W.; Wang, S.; Wang, S.; Yu, J.; Wang, J.; Yong, Q.; Chu, F.; Lu, C. Self-strengthening and conductive cellulose composite hydrogel for high sensitivity strain sensor and flexible triboelectric nanogenerator. *Int. J. Biol. Macromol.* **2023**, *248*, 125900. [CrossRef] [PubMed]

125. Ullah, R.; Shah, L.A.; Khan, M.T. Cellulose nanocrystals boosted hydrophobically associated self-healable conductive hydrogels for the application of strain sensors and electronic devices. *Int. J. Biol. Macromol.* **2024**, *260*, 129376. [CrossRef] [PubMed]

126. Meng, L.; Li, W.; Ding, S.; Liu, E.; Liu, D. Preparation and properties of polyacrylamide/cellulose nanocrystal/reduced graphene oxide interpenetrating network composite hydrogels. *New J. Chem.* **2023**, *47*, 14273–14281. [CrossRef]

127. Xu, A.; Xia, Q.; Ju, Y.; Wang, Y.; Xiao, Z.; Wang, H.; Xie, Y. Cellulose enhanced highly sensitive and durable dual-network ionogel sensor for human motion monitoring. *Chem. Eng. J.* **2024**, *499*, 156608. [CrossRef]

128. Fu, D.; Xing, L.; Xie, Y.; Li, P.; Yang, F.; Sui, X.; Liu, J.; Chi, J.; Huang, B.; Shen, J. Hybrid crosslinking cellulose nanofibers-reinforced zwitterionic poly (ionic liquid) organohydrogel with high-stretchable, anti-freezing, anti-drying as strain sensor application. *Carbohydr. Polym.* **2025**, *353*, 123253. [CrossRef]

129. Fu, D.; Xing, L.; Xie, Y.; Shen, J. High-mechanical properties, anti-freezing, and self-regeneration zwitterionic poly (ionic liquid) hydrogel reinforced by cellulose nanofibers for strain sensor applications. *Int. J. Biol. Macromol.* **2025**, *320*, 145999. [CrossRef] [PubMed]

130. Rong, X.; Ding, Q.; Chen, L.; Yang, S.; Lou, J.; Liu, Z.; Li, X.; Jiang, Y.; Wang, X.; Han, W. Hyper strength, high sensitivity integrated wearable signal sensor based on non-covalent interaction of an ionic liquid and bacterial cellulose for human behavior monitoring. *Mater. Horiz.* **2024**, *11*, 2420–2427. [CrossRef]

131. Zhou, Y.; Wang, L.; Liu, Y.; Luo, X.; He, Y.; Niu, Y.; Xu, Q. Transparent, stretchable, self-healing, and self-adhesive ionogels for flexible multifunctional sensors and encryption systems. *Chem. Eng. J.* **2024**, *484*, 149632. [CrossRef]

132. Li, T.; Liu, J.; Shu, H.; Sun, A.; Zhao, T.; Chen, Y.; Chen, Y. High-Performance Deep Eutectic/Ionic Liquid Gels for Zinc-Ion Battery and Flexible Sensor Applications in Extreme Environments. *Adv. Funct. Mater.* **2025**, e14358. [CrossRef]

133. Lu, C.; Guo, X.; Wang, C.; Wang, J.; Chu, F. Integration of metal-free ATRP and Diels-Alder reaction toward sustainable and recyclable cellulose-based thermoset elastomers. *Carbohydr. Polym.* **2020**, *242*, 116404. [CrossRef]

134. Zhu, S.; Sun, H.; Lu, Y.; Wang, S.; Yue, Y.; Xu, X.; Mei, C.; Xiao, H.; Fu, Q.; Han, J. Inherently conductive poly (dimethylsiloxane) elastomers synergistically mediated by nanocellulose/carbon nanotube nanohybrids toward highly sensitive, stretchable, and durable strain sensors. *ACS Appl. Mater. Interfaces* **2021**, *13*, 59142–59153. [CrossRef]

135. Xu, S.; Jia, Q.; Zhang, K.; Lu, C.; Wang, C.; Wang, J.; Yong, Q.; Chu, F. Recyclable and mechanically tough nanocellulose reinforced natural rubber composite conductive elastomers for flexible multifunctional sensor. *Int. J. Biol. Macromol.* **2024**, *268*, 131946. [CrossRef] [PubMed]

136. Xu, M.; Yue, Y.; Lu, Y.; Xiang, K.; Wang, J.; Lu, W.; Tian, H.; Jia, L.; Wu, G.; Xiao, J. Three-dimensional printed cellulose nanofibers/carbon nanotubes/silicone rubber flexible strain sensor for wearable body monitoring. *J. Mater. Chem. C* **2024**, *12*, 5972–5984. [CrossRef]

137. Lu, Y.; Yue, Y.; Ding, Q.; Mei, C.; Xu, X.; Jiang, S.; He, S.; Wu, Q.; Xiao, H.; Han, J. Environment-tolerant ionic hydrogel–elastomer hybrids with robust interfaces, high transparence, and biocompatibility for a mechanical–thermal multimode sensor. *InfoMat* **2023**, *5*, e12409. [CrossRef]